# Single-cell analysis characterizes PLK1 as a catalyst of an immunosuppressive tumor microenvironment in LUAD

**Yifan Kong[1, 5], Chaohao Li[1, 5], Jinpeng Liu[3, 5], Min Zhang[1], Derek B. Allison[4], Faisal Hassan[4], Daheng He[3], Xinyi Wang[1], Fengyi Mao[1], Qiongsi Zhang[1], Yanquan Zhang[1], Zhiguo Li[1], Sai Wu[1], Chi Wang[2, 3] and Xiaoqi Liu[1, 3*]**

[1]Department of Toxicology and Cancer Biology, University of Kentucky, Lexington, KY, 40536

[2]Department of Biostatistics, University of Kentucky, Lexington, KY, 40536

[3]Markey Cancer Center, University of Kentucky, Lexington, KY, 40536

[4]Department of Pathology and Laboratory Medicine, University of Kentucky, Lexington, KY, 40536

[5]These authors contribute equally.

**Running title:** PLK1 promotes immunosuppressive TME.

**Keywords:** PLK1, LUAD, TME, single-cell RNA-seq, TAM, MHC-II.

**Conflict of Interest:** The authors declare no conflict of interest.

*** To whom correspondence should be addressed:**

Dr. Xiaoqi Liu: Department of Toxicology and Cancer Biology, University of Kentucky, Lexington, KY, 40536. Phone: 859-562-2006; Fax: 859-323-1059; Email: xiaoqi.liu@uky.edu

**Abstract**

PLK1 (Polo-like kinase 1) plays a critical role in the progression of lung adenocarcinoma (LUAD). Recent studies have unveiled that targeting PLK1 improves the efficacy of immunotherapy, highlighting its important role in the regulation of tumor immunity. Nevertheless, our understanding of the intricate interplay between PLK1 and the tumor microenvironment (TME) remains incomplete. Here, using genetically engineered mouse model and single-cell RNA-seq analysis, we report that PLK1 promotes an immunosuppressive TME in LUAD, characterized with enhanced M2 polarization of tumor associated macrophages (TAM) and dampened antigen presentation process. Mechanistically, elevated PLK1 coincides with increased secretion of CXCL2 cytokine, which promotes M2 polarization of TAM and diminishes expression of class II major histocompatibility complex (MHC-II) in professional antigen-presenting cells. Furthermore, PLK1 negatively regulates MHC-II expression in cancer cells, which has been shown to be associated with compromised tumor immunity and unfavorable patient outcomes. Taken together, our results reveal PLK1 as a novel modulator of TME in LUAD and provide possible therapeutic interventions.

## Introduction

Lung cancer accounts for one-fifth of all cancer mortalities in the US, making it the leading cause of cancer-related deaths [1]. Lung adenocarcinoma (LUAD) is the major type of this disease, comprising almost half of all cases [2]. LUAD is characterized by a myriad of genetic alternations that drive tumor heterogeneity, such as the common mutation forms involved in receptor tyrosine kinase pathways including EGFR, KRAS, ALK, and ROS1 genes [3]. These mutations exert a profound influence on disease progression and wield considerable sway over patients' responses to treatment. As a result, a slew of targeted therapies has emerged, tailored to the unique genetic profiles of individual patients. Despite the advances in treatment options, the outlook for LUAD remains dishearteningly bleak, with the 5-year survival rate for metastatic disease is less than 5%. Therefore, precise early screening and the development of more efficacious treatment modalities are essential to improve patients' outcomes.

Recently, immunotherapies have emerged as a novel treatment option for LUAD [4]. While this marks the new era of cancer treatment, the success of immunotherapies depends on several factors, including the patient's immune status, and most importantly, the characteristics of the tumor microenvironment (TME), which has emerged as a pivotal area of cancer research [5]. TME is composed of various types of tumor-infiltrating myeloid cells and lymphocytes, and the interactions between cancer cells and these immune cells shape the properties of multiple cancer hallmarks, such as tumor growth, invasion, and metastasis. More closely, immunosuppressive TME can render immunotherapies ineffective, and this nature accounts for the fact that most cancer patients don't respond to immunotherapy [6]. Within the realm of lung cancer, only 20% of patients respond to monotherapy with checkpoint blockade, a figure that modestly escalates to 40% when paired with conventional chemotherapy [7, 8], underscoring a more complex yet

79 underexplored features of TME in LUAD. Therefore, a better understanding of the TME holds
80 paramount importance in developing effective immunotherapies.

81 Polo-like kinase 1 (PLK1) emerges as a pivotal serine/threonine kinase, orchestrating a multitude
82 of crucial cellular processes. Its canonical function takes center stage in the intricate regulation of
83 cell division across multiple phases [9-14]. Beyond its canonical role, studies have unveiled its
84 participation in non-mitotic functions, including the regulation of DNA damage repair, metabolism,
85 and immune response [15]. Dysregulation of PLK1, characterized by heightened expression levels,
86 has been identified as a pivotal player in the initiation and progression of various cancer types [16].
87 Considering its importance in tumorigenesis, novel therapies targeting PLK1 have been developed
88 with observable efficacy in cell and animal models [17]. Both our lab and others have proven that
89 PLK1 overexpression in LUAD leads to cancer progression and is associated with poor overall
90 survival [18, 19]. Interestingly, recent studies have validated PLK1 as a potential target to improve
91 the efficacy of immunotherapies in lung cancer [20], consistent with our finding in pancreatic
92 cancer that targeting PLK1 in pancreatic cancer enhances the effectiveness of immune checkpoint
93 blockade [21]. While these results suggest that PLK1 may be an important modulator of tumor
94 immunity, whether and how PLK1 functions in the TME of LUAD is largely unknown. Here,
95 using single-cell sequencing, we show that elevation of PLK1 incurs a suppressive TME in LUAD,
96 marked by M2 polarization of tumor associated macrophages (TAM) and suppression of antigen
97 presentation process. In addition, elevation of PLK1 attenuates the expression of class II major
98 histocompatibility complex (MHC-II) in professional antigen presentation cells and cancer cells,
99 leading to impaired antigen presentation and anti-tumor immunity. Overall, our results reveal
100 PLK1 as a key regulator of TME and provide evidence of targeting PLK1 to improve
101 immunotherapies in LUAD.

102 **Materials and Methods**

103 Antibodies, chemicals, and siRNA can be found in **Table S7**.

104 **Sample preparation for single-cell sequencing**

105 All animal experiments used in this study were approved by the University of Kentucky Division
106 of Laboratory Animal Resources. 8-week-old LSL-Kras$^{G12D}$/Tp53$^{f/f}$ (KP) and LSL-
107 Kras$^{G12D}$/Tp53$^{f/f}$/LSL-Plk1 (KPP) mice were intratracheally instilled with adenovirus-expressing
108 Cre recombinase (Ad-Cre) at a viral titer of $2.5 \times 10^7$ PFU per mouse according to the protocol
109 [22]. Tumor formations were monitored every week by MRI and harvested after 12 weeks of
110 adenovirus delivery. Single cell suspensions were prepared following 10x Genomics Cell
111 Preparation Guide. Briefly, mice lung tissues were harvested and cut into smaller pieces, then used
112 pipette to extensively pipette up and down to get tissue mixture in DMEM medium containing 2%
113 FBS. This mixture was filtered with a 70 μm nylon mesh strainer, centrifuged at 300g for 10 mins,
114 then resuspended in DMEM medium containing 2% FBS to get single cell suspension. The single
115 cell suspension was further sorted to enrich immune cell populations, and this suspension was
116 processed for single-cell sequencing. Cell viability was at least 95% for all samples. 10000 cells
117 were targeted for sequencing and loaded onto a Chromium Controller (10x Genomics) for gel
118 beads-in-emulsion formation. Library preparation was conducted using Chromium Next GEM
119 Single Cell 3' Gene Expression Kit (v3.1, 10x Genomics) according to the manufacturer's
120 instructions. Single indexed, paired-end libraries were sequenced on an HiSeq 2500 sequencer
121 (Illumina).

122

123

124 **Analysis of single-cell RNA-seq**

125 Single-cell RNA-seq gene expression libraries were mapped to mm10 mouse reference (10x
126 Genomics pre-built reference, mm10-2020-A) using Cell Ranger (v6.1.1, 10x Genomics). For each
127 library, Cell Ranger filtered matrix was subjected to QC filters to remove low quality cells with
128 $\leqslant$ 500 features or percentage of mitochondrial transcripts $\geqslant$ 15. DoubletFinder analysis was then
129 performed on each library separately to identify and filter potential doublets with default
130 parameters [23]. Additionally, cells with features > 8000 or counts > 50,000 were removed. Pass
131 QC cells from the KP and KPP groups were combined and processed using the Seurat (v3) R
132 package [24]. Count matrices were Log-normalized and scaled. The top 2,000 highly variable
133 genes (HVGs) were selected to define principal components (PCs). Batch integration was
134 performed via Harmony algorithm (v0.1.0) to the combined data for batch effect corrections with
135 default settings [25]. Neighbor analysis was performed by FindNeighbors function using the PCs
136 from the Harmony dimension. Clustering was identified with FindClusters function at resolution
137 = 0.8. UMAP was calculated based on the Harmony dimension for clusters visualization.
138 Identification of cluster markers was performed using a Wilcoxon rank-sum test by comparing
139 each cluster with the rest of the cells. The two-sample binomial test will be used to compare the
140 distribution of cell clusters between the two groups. For differential gene expression analysis, we
141 used DESeq2 test in Seurat [26], to identify the up/down-regulated sets of genes between treatment
142 groups in the cell populations. Gene Set Enrichment Analysis (GSEA) was performed with fgsea
143 R package [27], using KEGG and HALLMARK datasets [28, 29].

144

145

146 **Analysis of public dataset and bulky RNA-seq**

147 For STRING analysis [30], genes functionally associated with CXCL2 were directly checked with
148 online STRING tool (https://string-db.org/). For gene expression, correlation, and survival
149 analyses of TCGA-LUAD dataset, patients' demographic data with RSEM and zscore values
150 (normalized to all samples) of RSEM were downloaded from cBioportal [31-33]. Analysis of
151 bulky RNA-seq data from KP and KPP tumors was described previously [19].

152 **Cell culture**

153 KP and KPP cell lines were isolated from transgenic mice 12–14 weeks after adenovirus infection,
154 which was described before [19]. H358 cell line was purchased from ATCC (CRL-5807). All cell
155 lines were cultured in RPMI 1640 medium containing 10% FBS, 1% penicillin-streptomycin at
156 37°C incubator with 5% $CO_2$. For preparation of conditioned medium, KP or KPP cells were
157 cultured in 100mm dishes until 70-80% confluency, then medium was refreshed with DMEM
158 medium containing 0.5% FBS and continued to culture for 48 hours. The resulting conditioned
159 medium was used for coculture experiments and mouse cytokine array. For transfection of siRNA,
160 predesigned siRNA (Sigma) targeting PLK1 were transfected with jetPRIME Versatile
161 DNA/siRNA transfection reagent (Polyplus, 101000001) according to the manufacturer's
162 instructions. 48 hours after transfection, cells were harvested for subsequent experiments. All the
163 cell lines were within 50 passages and tested negative for mycoplasma contamination.

164 **Coculture experiments**

165 Macrophages and dendritic cells were isolated from the bone marrows of B6 hosts. Briefly, bone
166 marrows were flushed out of the femur and tibia with complete DMEM medium using 25-gauge
167 needles. After centrifugation at 400g for 5 mins, bone marrows suspension was treated with 1x

168 RBC lysis buffer (Thermo, 00-4333-57) and centrifuged again. The cell pellets were then washed
169 with 1x PBS twice and resuspended in refresh complete DMEM medium. Cells were cultured at
170 37°C incubator with 5% $CO_2$ for a week to induce differentiation. For induction of macrophages,
171 cells were treated with 10ng/ml Csf1. For induction of dendritic cells were treated with 10ng/ml
172 Csf2 and 20ng/ml Il-4. Medium with cytokines was refreshed every two days. For coculture with
173 cells, KP or KPP cells were directly seeded onto the same plates containing immune cells at
174 indicated ratio for 48 hours. Treatment with Cxcl2 or SX-682 started at 6 hours post coculture and
175 continued until end of the experiments. For coculture with conditioned medium, the conditioned
176 medium from KP or KPP, with mouse IgG or anti-Cxcl2 neutralization antibodies, was used to
177 replace normal culture medium for immune cells and continued to culture for 48h.

178 **Flow cytometry**

179 Cells were harvested by a cell scraper and washed once with 1x PBS, then stained on ice with
180 indicated antibodies (1:1000) in 1x PBS for 30 mins. Samples containing tumor cells were fixed
181 with 70% ethanol before staining. Data were acquired on the BD Symphony A3 analyzer (BD
182 Biosciences) and analyzed using FlowJo software (BD Biosciences).

183 **Mouse cytokines array**

184 Mouse cytokine array experiment was performed using Proteome Profiler Mouse Cytokine Array
185 Kit (R&D Systems, ARY006) according to the manufacturer's instructions. Briefly, conditioned
186 medium from KP and KPP was incubated with membranes containing pre-adsorbed primary
187 antibodies targeting mouse cytokines. Following wash step, the membranes were then incubated
188 with HRP-linked secondary antibodies. After washing membranes again, membranes were probed
189 with chemiluminescent reagents to visualize cytokine spots. Medium containing 0.5% FBS but

190 without cancer cells was used as negative control. Images were captured with ChemiDoc Imaging
191 System (Bio-Rad) and analyzed with Image Lab software (Bio-Rad).

192 **Immunohistochemistry (IHC)**

193 Formalin-fixed, paraffin-embedded slides prepared from KP and KPP tumors were stained with
194 MHC-II antibodies. IHC staining was performed with the VECTASTAIN Elite ABC Universal
195 PLUS Kit (Vector Laboratories, PK-8200) according to the manufacturer's instructions. Staining
196 was visualized with ImmPACT DAB Substrate Kit (Vector Laboratories, SK-4105) and
197 counterstained with Harris's hematoxylin. Images were with the Nikon microscope.

198 **Statistical analysis**

199 Statistical analyses were performed with the statistical functions in GraphPad Prism 8 and R
200 programming language. Unless denoted elsewhere, an unpaired two-sided t test was used as the
201 default method for results. Normality and variance of results were checked to confirm the
202 requirements of t test. Statistical significance was set at $p < 0.05$ unless denoted otherwise.

203

204 **Results**

205 **Elevation of PLK1 is associated with immunosuppressive TME in LUAD.**

206 To investigate the impact of PLK1 on lung cancer TME, we designed a workflow to perform the
207 single-cell RNA-seq using our LSL-Kras$^{G12D}$/Tp53$^{f/f}$ (KP) and LSL-Kras$^{G12D}$/Tp53$^{f/f}$/LSL-Plk1
208 (KPP) mouse models (**Fig. 1A**), which were previously reported [19]. Using the markers to
209 differentiate non-immune and immune cells (**Figs. S1A-S1B**), the results showed that most cells
210 (over 95%) were captured as immune cells without significant differences in KP and KPP groups

211 (**Fig. S1C**), demonstrating the efficacy and reliability of single-cell data to characterize TME in
212 both groups. Unsupervised clustering of immune cells generated 20 different immune cell clusters
213 in samples characterized by a specific gene signature (**Figs. S1D-S1E, Table S1**), indicating a
214 significant intratumoral heterogeneity of immune cell populations. Notably, the different
215 proportions of immune cell clusters suggested a distinct TME in KP and KPP (**Figs. S1F-S1G**).
216 To better visualize the differences in immune cell populations, we performed a supervised
217 clustering of major immune cell types based on their specific gene signatures (**Figs. 1B-1C, Table**
218 **S2**). Results showed that KPP tumors had significantly lower proportions of all cell types except
219 for TAM compared to KP tumors (**Figs. 1D-1E**). In both groups, TAM were the major population,
220 suggesting the unique function of them in lung cancer progression. Besides, the lower levels of
221 tumor-infiltrating lymphocytes (B cells and T cells) in KPP tumors indicated an
222 immunosuppressive TME in this group. Since T cells and NK cells are the major immune cells
223 exerting direct anti-tumor immunity, we further investigated these populations by clustering them
224 in KP and KPP tumors (**Figs. S2A-S2B, Table S3**). Clearly, KPP tumors displayed decreased
225 proportions of tumor-infiltrating NK cells and T cells of all subtypes (**Fig. S2C**). The lower levels
226 of these tumor-infiltrating lymphocytes in KPP tumors were impactful and further supported a cold
227 TME in this group, as they were the major immune cells responsible for eliminating tumors. This
228 observation suggested that KPP tumors were specifically protected from the anti-tumor immunity
229 and thus resistant to the host immune defense. Taken together, these results illustrated that high
230 PLK1 in LUAD promoted a suppressive immunophenotype.

231

232

233

234 **Tumor-promoting M2 macrophages propagate in high-PLK1 TME of LUAD.**

235 The relatively higher proportion of TAM in KPP tumors was intriguing, and this phenomenon
236 enticed us to investigate the role of TAM in high-PLK1 TME. Given that the functions of TAM
237 were dichotomous, we specially focused on the proportions of M1 and M2 macrophages in KP
238 and KPP tumors, which were tumor-suppressing and tumor-promoting, respectively. Analysis of
239 gene expressions in TAM identified 1201 differentially expressed genes with statistical
240 significance between KP and KPP tumors (**Fig. 2A, Table S4**). Investigation of top 10 up and
241 down regulated genes in KPP group revealed that TAM in KPP tumors were positively enriched
242 for genes associated with M2 macrophages (e.g., Chil3, Ccn3) while negatively enriched for genes
243 associated with M1 macrophages (e.g., H2-Eb1, H2-Ab1), suggesting that TAM in KPP tumors
244 were more enriched for M2 subtype (**Fig. 2B**). Comparison of M1 gene signature and M2 gene
245 signature in KP and KPP groups further supported increased M2 macrophages in KPP tumors (**Fig.
246 2C, Table S5**). To confirm this phenotype, we performed supervised clustering of total
247 macrophages (**Figs. 2D-2E, Table S5**), and the results indeed demonstrated that TAM in KPP
248 tumors consisted of more M2 macrophages compared to KP tumors (**Figs. 2F**). Since M2
249 macrophages were considered tumor-promoting and immunosuppressive, the higher proportion of
250 M2 macrophages in KPP tumors was consistent with a colder TME in this group. In sum, these
251 results supported the notion that high PLK1 was associated with increased tumor-promoting M2
252 macrophages in LUAD.

253

254

255

256 **High PLK1 suppresses antigen presentation pathway and induces M2 polarization.**

257 Since high PLK1 was associated with increased infiltration and differentiation of M2 macrophages,
258 we sought to delineate the biological consequence of this phenotype. To achieve this aim, we
259 performed GSEA in TAM. The results showed that multiple pathways associated with the
260 functions of macrophages were dramatically disturbed (**Fig. 3A, Table S6**). Several pathways
261 related to immune response were suppressed in KPP tumors, such as pathways associated with
262 inflammation (e.g., IFN-γ response, **Fig. 3B**), pathogen defense (e.g., viral myocarditis), and
263 autoimmune diseases (e.g., systemic lupus erythematosus). In addition, pathways associated with
264 steroid and lipid metabolism were elevated in KPP tumors (e.g., steroid biosynthesis, **Fig. 3B**),
265 which were previously demonstrated to promote M2 polarization [34]. These results suggested an
266 impaired anti-tumor immune defense and were in congruent with the observations of more M2
267 macrophages and a more immunosuppressive phenotype in KPP tumors. Of note, antigen
268 processing and presentation pathway was among the most suppressed pathway in TAM (**Figs. 3A-**
269 **3B, Table S6**). Professional antigen presentation cells such as macrophages rely on MHC-II and
270 costimulatory factors for their antigen processing and presentation function. Indeed, review of
271 gene expressions and macrophages markers (**Figs. 2A-2C, Table S4, Table S5**) showcased that
272 some low-expression M1 genes in TAM of KPP tumors were also MHC-II genes (e.g., Cd74, H2-
273 Eb1, H2-Ab1, H2-Aa) and costimulatory factors (e.g., Cd86, Cd80), consistent with the impaired
274 antigen presentation function in TAM. Given that this pathway was key to successful anti-tumor
275 immunity [35], the loss of antigen presentation function in TAM and more tumor-promoting M2
276 macrophages in KPP group supported the immunosuppressive role of PLK1. Moreover, results of
277 GSEA in other immune cells showed that dampened antigen processing and presentation was a
278 shared consequence among immune cell populations (**Fig. S3, Table S6**), suggesting that

279 suppression of this critical pathway was a general consequence of high PLK1 expression. Based
280 on these results, we hypothesized that PLK1 could inhibit antigen presentation pathway, and this
281 led to M2 polarization. To validate our hypothesis, we performed in vitro coculture experiments
282 using established cell lines from KP and KPP mice and used flow cytometry to monitor expressions
283 of important genes and markers in antigen presentation and macrophages polarization **(Figs. 3C-**
284 **3D)**. Short-term coculture of bone marrow derived macrophages (BMDM) with KP or KPP
285 showed that both cells elevated costimulatory factors (Cd80 and Cd86) with even stronger effect
286 from KPP group. However, only KPP cells were able to induce higher level of M2 marker Cd206,
287 indicating the M2 polarization effect of PLK1. Coculture with both cell lines attenuated MHC-II
288 expression, possibly due to the immune suppression mechanism of tumors. Compared to KP, the
289 level of MHC-II was lower in KPP group. Given that MHC-II plays a pivotal role in antigen
290 processing and presentation, the lower expression of MHC-II in KPP group confirmed that antigen
291 presentation function was specifically dysregulated in high PLK1 condition. Collectively, these
292 data demonstrated that PLK1 suppressed antigen presentation pathway and induced M2
293 polarization in LUAD.

294

295 **Immunosuppressive function of PLK1 depends on CXCL2.**

296 Paracrine signaling through the release of cytokines from cancer cells is critical for intercellular
297 communication and shaping anti-tumor immunity [36]. Inspection of pathway analysis in TAM
298 (**Fig. 3A, Table S6**) revealed that several cytokine and chemokine pathways were altered (e.g.,
299 interferon response pathway), and this led to our hypothesis that PLK1 exerted its
300 immunosuppressive function via regulation of cytokine secretion. To test our hypothesis, we
301 performed a cytokines array of mouse cytokines released from the conditioned medium of KP and

302 KPP cells. We found that cytokine profiles were indeed different between KP and KPP. Compared
303 to KP, KPP cells secreted more Il-6, Cxcl2 and Ccl3 cytokines, but less Ccl5 (**Fig. 4A**). The
304 increased secretion of Il-6 was reasonable given its established role in M2 polarization [37].
305 Besides, Ccl3 (macrophage inflammatory protein 1-alpha) was one of the cytokines released from
306 macrophages and Ccl5 was responsible for T cells chemotaxis [38, 39], so their alternations were
307 congruent with the higher proportion of macrophages and lower infiltration of T cells in KPP
308 tumors. Among them, we were especially interested in Cxcl2, as it was the most highly secreted
309 cytokine in the supernatant of KPP. It has been shown that secreted CXCL2 in TME can recruit
310 myeloid derived suppressor cells and M2 macrophages [40, 41]**,** and this leads to suppression anti-
311 tumor response (**Fig. 4B**). We also investigated which pathway was responsible for the increased
312 secretion of Cxcl2 in KPP. A preliminary STRING analysis in human and mice identified several
313 important genes related to CXCL2 (**Figs. S4A**). Except for some known interaction genes (e.g.,
314 CXCR1 and CXCR2, two receptors for CXCL2), we found that in both species the genes related
315 to JAK-STAT3 pathway (e.g., IL6/Il6) and NFKB pathway (e.g., TNF, Rela) commonly emerged.
316 GSEA of RNA-seq data confirmed that two pathways were highly active in KPP cells (**Fig. S4B**).
317 Of note, although not very striking, Il-6 was simultaneously detected with Cxcl2 in the secretion
318 profile of KPP, which was not observed in KP control (**Fig. 4A**). These results provided evidence
319 that IL-6/JAK/STAT3 and TNF/NFKB axis might account for the increased Cxcl2 in KPP cells.

320 In mice, Cxcl2 can bind to Cxcr1 and Cxcr2, albeit with much higher affinity to Cxcr2 [42]. Given
321 that Cxcl2 was predominant in KPP-secreted cytokines and its established role in recruiting M2
322 macrophages, we hypothesized that the observed immunosuppressive function of PLK1 depended
323 on CXCL2. To test this assumption, we performed coculture experiments of BMDM with
324 conditioned medium from KP or KPP (Figs. 4C-4D), treated with recombinant mouse Cxcl2 or

325 SX-682, a previously reported dual CXCR1/CXCR2 inhibitor in clinical trial [43]. Coculture of
326 BMDM with conditioned medium recapitulated most of the results from coculturing with cells,
327 but MHC-II was not decreased. Instead, MHC-II elevated under this condition, indicating that the
328 decrease of MHC-II in coculture with cells directly came from interaction between cancer cells
329 and immune cells. Coculture with conditioned medium still elevated Cd80 and Cd86 in both
330 groups, with a much higher induction of M2 marker Cd206 in KPP group. Intriguingly, the
331 addition of Cxcl2 in conditioned medium from KP was able to reduce Cd80 and Cd86 while
332 increasing the level of Cd206. Besides, adding CXCR1/CXCR2 inhibitor in conditioned medium
333 from KPP group elevated Cd80 and Cd86 but attenuated Cd206 expression. However, MHC-II
334 was not disturbed by either Cxcl2 or SX-682. Considering that mouse Cxcl2 binds to Cxcr2 with
335 much higher affinity, and mouse Cxcr1 is mainly for Cxcl6 [42], the off-target effect of SX-682
336 in our experimental setting could be ignored. To address this issue, we performed a parallel
337 coculture experiment of BMDM with conditioned medium from KP and KPP (**Figs. 4E-4F**),
338 treated with mouse IgG control or anti-Cxcl2 neutralization antibodies. Treatment with
339 neutralization antibodies witnessed an uptrend of Cd80 and Cd86 but a downtrend of Cd206, with
340 an unchanged status of MHC-II, reassuring the results obtained from the coculture experiment
341 using SX-682. These data illustrated that Cxcl2 was partially responsible for the effect of PLK1 in
342 suppressing antigen presentation and inducing M2 polarization, mainly focused on regulation of
343 costimulatory factors. As costimulatory factors in professional antigen presentation cells, the
344 functions of CD80 and CD86 were similar in dendritic cells, and CD206 was also a hallmark of
345 immature dendritic cells with incomplete immune functions [44]. Thus, detection of these markers
346 in dendritic cells has similar value in dissecting the biological effect of PLK1 and CXCL2 on
347 antigen presentation. Thus, we repeated all three coculture experiments with dendritic cells

348 isolated from bone marrow. The results revealed that alternations of Cd80, Cd86 and Cd206 were
349 quite similar and repeatable, but the level of MHC-II displayed distinct changes. In the coculture
350 experiment with KP/KPP cells and dendritic cells, an increased proportion of KP cells
351 accompanied an elevated level of MHC-II, but an increased ratio of KPP cells reduced MHC-II
352 expression (**Figs. S5A-S5B**). This was different from the results in BMDM, where a higher ratio
353 of both cell lines was associated with a lower level of MHC-II. However, in both settings, KPP
354 cells were capable of diminishing MHC-II expression more strongly compared to KP, suggesting
355 PLK1's universal suppression of antigen presentation by limiting MHC-II expression. In the
356 coculture experiment with KP/KPP conditioned medium and dendritic cells, the results
357 demonstrated that the effect of PLK1 on MHC-II could be explained by CXCL2, as treatment with
358 Cxcl2 in KP group reduced MHC-II expression and treatment with either SX-682 or neutralization
359 antibodies in KPP group elevated MHC-II level (**Figs. S5C-S5F**), which was different from the
360 results in macrophages. Despite these differences, the disturbance of antigen presentation and
361 induction of immunosuppressive environment by CXCL2 was observed. Taken together, these
362 results stated that CXCL2 accounted for the immunosuppressive function of PLK1 in LUAD, but
363 the actual effect of CXCL2 might vary in different immune cells.

364

365 **PLK1 negatively regulates MHC-II in cancer cells.**

366 It has been reported that MHC-II can also express on the surface of cancer cells, and this phenotype
367 is associated with improved response to immunotherapy and better survival of cancer patients [45-
368 48]. However, this phenotype was unexplored in lung cancer. Based on these established facts and
369 our observations that PLK1 was negatively associated with MHC-II, we aimed to explore whether
370 PLK1 affected the expression of MHC-II in LUAD tumors. We first detected MHC-II expression

371 by IHC staining on tumor slides prepared from KP and KPP mice, and the results indeed showed
372 that both tumors expressed MHC-II, with more striking expression in KP tumors (**Fig. 5A**). This
373 was consistent with the results observed in immune cells that high PLK1 led to lower MHC-II
374 level. Next, we performed flow cytometry analysis of MHC-II level in KP and KPP cell lines, and
375 the results verified the lower expression of MHC-II in KPP cells (**Figs. 5B-5C**). Since MHC-II
376 expression in cancer cells depends on the IFN-γ [49], we performed ELISA experiment to detect
377 intracellular IFN-γ levels between KP and KPP cells. As expected, KPP cells had a lower level of
378 IFN-γ compared to KP (**Fig. 5D**), consistent with its inferior expression of MHC-II. To direct
379 assess the effect of PLK1, we treated KP and KPP with three PLK1 inhibitors (PLKi), including
380 BI-2536 (BI), GSK461364A (GSK) and Onvansertib (ONV). In both cells, treatment with PLK1i
381 consistently elevated the level of MHC-II (**Figs. 5E-5H**), confirming the negative regulation of
382 MHC-II by PLK1. To assess the human side, we utilized human H358 LUAD cell line to see
383 whether PLK1 played a similar role. We first transfected H358 cells with siRNA targeting PLK1,
384 and the depletion of PLK1 elevated MHC-II as expected (**Figs. 5I-5J**). Dose escalation of PLKi
385 also showed a gradual increase in MHC-II expression (**Figs. 5K-5L**), reassuring the effect of PLK1.
386 Cumulatively, these data supported the conclusion that PLK1 also regulated MHC-II in LUAD
387 cancer cells.

388

389 **Clinical assessment of PLK1's regulation of MHC-II**

390 We've previously demonstrated that high PLK1 was associated with worse patients' outcomes
391 [19], and this was consistent with the data that PLK1 suppressing MHC-II presented in this study.
392 To evaluate the translational values of our findings, we analyzed the TCGA-LUAD dataset. We
393 found that high PLK1 was associated with low levels of MHC-II member genes (**Figs. 6A, S6**).

394 Using this MHC-II gene signature, we calculated the MHC-II signature scores of all patients and
395 used these signature scores to re-classify patients into high MHC-II and low MHC-II groups, then
396 performed survival analysis of those patients. We found that patients with high MHC-II scores had
397 better survival outcomes compared to patients with low MHC-II scores (**Fig. 6B**). These results
398 were consistent with our previous findings and supported the notion that the negative regulation
399 of MHC-II by PLK1 may promote LUAD progression and result in poor outcomes. In conclusion,
400 PLK1 was negatively associated with MHC-II in clinical situations, and this had an impact on
401 patients' survival possibly through suppressing antigen presentation pathway.

402

403 **Discussion**

404 Here in this study, we render pioneering data to support the fact that PLK1 promoted an
405 immunosuppressive TME in LUAD (**Fig. 7**). Under low PLK1 condition, TME is characterized
406 by a higher proportion of tumor infiltrating lymphocytes and lower level of CXCL2, and this
407 condition is associated with more M1 polarization and functional antigen presentation pathway. In
408 addition, tumors express more MHC-II and this feature is associated with better patient's survival.
409 Under high PLK1 condition, TME is characterized by low tumor infiltrating lymphocytes and high
410 secreted CXCL2, which promotes M2 polarization and disrupts antigen processing and
411 presentation. Tumors in this situation also express a lower level of MHC-II, which is associated
412 with worse outcomes of patients. The differences in TME shown in high PLK1 and low PLK1
413 conditions suggest that PLK1 is an important modulator of TME, and targeting PLK1 may be a
414 practical therapeutic intervention in LUAD treatment.

415 Although the emergence of immunotherapy has expanded the treatment options for lung cancer
416 patients, the efficacy is questionable due resistance to immunotherapy. Thus, identifying
417 mechanisms behind this harmful condition is urgently needed. Here, we report a novel mechanism
418 of PLK1 in cancer promotion. Previously, PLK1 has been largely considered as a canonical cell
419 cycle regulator in the past decades. However, recent studies have gradually uncovered the tumor-
420 promoting functions of this kinase. The fact that PLK1 suppresses anti-tumor in LUAD is
421 intriguing given that immunotherapy is one of the major therapeutic approaches for lung cancer.
422 The major reasons of resistance to immunotherapies are the scarcity of tumor-infiltrating immune
423 cells and existence of immune checkpoints [50]. We show that high PLK1 is associated with lower
424 infiltrating cytotoxic T cells and NK cells, and this feature is harmful to anti-tumor response in
425 LUAD. The decreased infiltration of T cells and NK cells may be due to the increased M2
426 polarization from TAM, which is a well-established suppressor of their functions. Besides,
427 functional antigen presentation in TME is the key to the success of anti-tumor immune response,
428 and immune evasion through suppressing this critical process significantly reduces the efficacy of
429 immunotherapy [35]. The novelty of our study lies in the fact we first demonstrate that PLK1
430 inhibits antigen presentation pathway by down regulating MHC-II in professional antigen-
431 presenting cells, which is the key molecule responsible for processing and presentation of tumor-
432 specific neoantigens. Besides, this conclusion can be extended to cancer cells, where high PLK1
433 is also associated with low MHC-II expression. The expression of MHC-II in tumors is a good
434 biomarker for better survival of patients [45-48]. However, the function of MHC-II in cancer cells
435 is unclear. Given that MHC-II is mainly responsible for antigen presentation, the fact that MHC-
436 II expressing in cancer cells may be involved in this process by functionally mimicking antigen
437 presentation process and priming CD4 T cells, which directly bind to MHC-II to activate immune

438 response, and this idea has been supported by the discovery of certain MHC-II specific neoantigens
439 in tumor cells and their necessities in promoting successful anti-tumor response [48]. Considering
440 the negative regulation of MHC-II by PLK1, our study further supports this notion in LUAD.
441 Despite that, the mechanistic part behind this regulation is missing and requires further exploration.

442 Considering the predominant immunosuppressive functions of PLK1 in LUAD and other cancer
443 types, treatment focuses on targeting PLK1 may decelerate tumor growth by boosting immune
444 response in TME. However, it is noteworthy that PLK1 may be negatively correlated with PD-L1
445 in certain situations [20, 21], devaluing the monotherapy with PLK1 inhibitor as this approach will
446 unexpectedly elevate immune checkpoints. Thus, combination treatment with PLKi and immune
447 checkpoints blockade should exhibit premium effect, and this assumption remains to be
448 investigated by future studies.

449

450

451

452

453

454

455

456

457

**Acknowledgement**

This study is supported by NIH R01 CA157429 (XL), R01 CA196634 (XL), R01 CA264652 (XL), R01 CA256893 (XL). This study is also supported by the Biospecimen Procurement & Translational Pathology, Biostatistics and Bioinformatics, Redox Metabolism, Flow Cytometry and Immune Monitoring Shared Resources, and OncoGenomics Shared Resource Facility of the University of Kentucky Markey Cancer Center (P30CA177558).

**Data availability**

All data are included in this article. Bulky RNA-seq data was deposited in GEO under accession number GSE206644.

**Figure 1. Single-cell RNA-seq analysis of KP and KPP mice.**

**A,** Workflow of single-cell RNA-seq of KP and KPP mice. **B,** Representative genes used for classification of T cells, B cells, Neutrophils, Dendritic cells, Macrophages. **C,** UMAP of major immune cell populations in KP and KPP. **D,** Comparison of cell populations between KP and KPP (n=3). **E,** Proportion of cell populations in KP and KPP. *, $p < 0.05$. **, $p < 0.01$. ***, $p < 0.001$.

496 **Figure 2. High PLK1 is associated with increased M2 macrophages.**

497 **A,** Volcano plot of differentially expressed genes (KPP vs KP, FDR < 0.05) in TAM. Top 10 up
498 and down regulated genes (ranked by $Log_2^{FC}$) are labeled. $Log_2^{FC}$, $Log_2^{fold\ change}$. **B,** Heatmap of
499 top 10 up and down regulated genes identified in A. **C,** Heatmap of top 50 representative genes
500 (ranked by $Log_2^{FC}$) in M1 and M2 gene signatures. **D,** Representative genes and functional markers
501 used for classification of M1 (Cd86, H2-Eb1) and M2 (Chil3, Pparg) macrophages. **E,** UMAP of
502 M1 and M2 macrophages in KP and KPP. **F,** Proportion of M1 and M2 macrophages in KP and
503 KPP.

504

505

506

507

508

509

510

511

512

513

514

515

516 **Figure 3. PLK1 suppresses antigen presentation pathway and promotes M2 polarization.**

517 **A,** Significant pathways (KPP vs KP, FDR < 0.1) altered in macrophages identified by GSEA.
518 NES, normalized enrichment score. **B,** GSEA plots of three exemplary pathways in A. **C,** Flow
519 cytometry analysis of indicated genes in BMDM cocultured with KP or KPP at the indicated ratio
520 for 48 hours. **D,** Quantification of C (n=3). *, $p < 0.05$. ***, $p < 0.001$.

521

522

523

524

525

526

527

528

529

530

531

532

533

534

535 **Figure 4. CXCL2 is responsible for the immunosuppressive function of PLK1.**

536 **A,** Cytokines array detection of cytokines secretion from the culture medium of KP and KPP.
537 Notable differences are labeled. **B,** Illustration of CXCL2's function in suppressing anti-tumor
538 immunity. **C,** Flow cytometry analysis of BMDM cocultured with conditioned medium from KP
539 or KPP for 48 hours, with or without recombinant Cxcl2 (2ug/ml) or CXCR1/CXCR2 inhibitor
540 SX-682 (1μM) treatment. **D,** Quantification of C (n=3). **E,** Flow cytometry analysis of BMDM
541 cocultured with conditioned medium from KP or KPP for 48 hours, with or without anti-Cxcl2
542 neutralization antibodies (5ug/ml) treatment. **F,** Quantification of E (n=3). *, $p < 0.05$. **, $p < 0.01$.
543 ***, $p < 0.001$.

544

545

546

547

548

549

550

551

552

553

554

555 **Figure 5. PLK1 suppresses MHC-II expression in tumor cells.**

556 **A,** Representative IHC images of KP and KPP tumors stained with MHC-II antibodies. **B,** Flow
557 cytometry detection of MHC-II in KP and KPP cells. **C,** Quantification of B (n=3). Data are
558 normalized to KP and shown as mean±SD. **D,** ELISA detection of IFN-γ in KP and KPP cells
559 (n=6). Data are normalized to KP and shown as mean±SD. **E,** Flow cytometry detection of MHC-
560 II in KP cells treated with PLK1 inhibitors (50nM BI, 50nM GSK, 200nM ONV) for 48 hours. **F,**
561 Quantification of E (n=3). Data are normalized to Ctrl and shown as mean±SD. **G,** Flow cytometry
562 detection of MHC-II in KPP cells treated with PLK1 inhibitors (50nM BI, 50nM GSK, 200nM
563 ONV) for 48 hours. **H,** Quantification of G (n=3). Data are normalized to Ctrl and shown as
564 mean±SD. For these results, an unpaired one-sided t test was used. **I,** Flow cytometry detection of
565 MHC-II in H358 cells 48 hours after transfection with siRNA control or siRNA targeting PLK1.
566 **J,** Quantification of I (n=3). Data are normalized to Ctrl and shown as mean±SD. **K,** Flow
567 cytometry detection of MHC-II in H358 cells with dose escalation of PLK1 inhibitor ONV (nM)
568 for 48 hours. **L,** Quantification of K (n=3). Data are normalized to untreated group (0) and shown
569 as mean±SD. *, $p < 0.05$. **, $p < 0.01$. ***, $p < 0.001$.

570

571

572

573

574

575

576 **Figure 6. Clinical evidence of PLK1 in suppressing MHC-II in lung cancer.**

577 **A,** Heatmap of MHC-II signature genes in TCGA-LUAD patients separated into high PLK1 and
578 low PLK1 groups. Patients are clustered based on the median expression (zsocres of $Log_2^{RSEM+1}$)
579 of PLK1. **B,** Survival curves of TCGA-LUAD patients separated into MHC-II high and MHC-II
580 low groups. $Log_2^{RSEM+1}$ of MHC-II signature genes in A are averaged to get signature scores.
581 Patients are clustered based on the median value of signature scores. For these results, a Log-rank
582 test was used.

583

584

585

586

587

588

589

590

591

592

593

594

595 **Figure 7. Summary of working model.**

596 Under low PLK1 condition, there is low level of CXCL2 secreted from tumors. Tumor
597 microenvironment is "hot", characterized by increased tumor infiltrating lymphocytes, M1
598 polarization of TAM and functional APC. Cancer cells are MHC-II high and this feature is
599 associated with better survival of patients. Under high PLK1 condition, there is increased secretion
600 of CXCL2 from tumors. Tumor microenvironment is "cold", characterized by low levels of tumor
601 infiltrating lymphocytes, M2 polarization of TAM and dysfunctional APC. Cancer cells are MHC-
602 II low and patients have worse survival outcomes.

603

604

605

606

607

608

609

610

611

612

613

614

615 **Figure S1. Single-cell RNA-seq analysis.**

616 **A,** Representative genes and functional markers used for classification of immune cells (Ptprc)
617 and non-immune cells (Krt18). **B,** UMAP of immune and non-immune cells in KP and KPP. **C,**
618 Comparison of immune and non-immune cells proportions between KP and KPP (n=3). **D,** UMAP
619 of immune cells undergoing unsupervised clustering in KP and KPP. **E,** Heatmap of top 5 signature
620 genes of each cluster in D. **F,** Proportions of unsupervised clusters in KP and KPP. **G,** Comparison
621 of unsupervised clusters proportions between KP and KPP. Statistical method: two-sample
622 binomial test. ***, FDR < 0.001.

623

624

625

626

627

628

629

630

631

632

633

634

635 **Figure S2. Single-cell RNA-seq analysis of T cell and NK cell populations.**

636 **A,** Representative genes used for identifying T cell and NK cell populations. **B,** UMAP projection
637 of T cell and NK cell populations. **C,** Comparison of proportions (in total immune cells) of T cell
638 and NK cell populations denoted in B between KP and KPP (n=3). *, $p < 0.05$. **, $p < 0.01$. ***,
639 $p < 0.001$.

640

641

642

643

644

645

646

647

648

649

650

651

652

653

654 **Figure S3. GSEA results of immune cell populations.**

655 Significant pathways (KPP vs KP, FDR < 0.1) in the indicated immune cell populations are shown.

656

657

658

659

660

661

662

663

664

665

666

667

668

669

670

671

672 **Figure S4. RNA-seq analysis of KP and KPP cells.**

673 **A,** STRING analysis of functional genes associated with CXCL2 in human and mice. **B,** GSEA
674 table of two potential pathways regulating CXCL2 secretion in KPP cells, identified by our
675 previously published RNA-seq data (GSE206644, KPP vs KP). FDR < 0.05 indicates a
676 significance.

677

678

679

680

681

682

683

684

685

686

687

688

689

690

691 **Figure S5. Coculture experiments of dendritic cells.**

692 **A,** Flow cytometry analysis of indicated genes in dendritic cells cocultured with KP or KPP at the
693 indicated ratio for 48 hours. **B,** Quantification of A (n=3). **C,** Flow cytometry analysis of dendritic
694 cells cocultured with conditioned medium from KP or KPP for 48 hours, with or without
695 recombinant Cxcl2 (2ug/ml) or CXCR1/CXCR2 inhibitor SX-682 (1μM) treatment. **D,**
696 Quantification of C (n=3). **E,** Flow cytometry analysis of dendritic cells cocultured with
697 conditioned medium from KP or KPP for 48 hours, with or without anti-Cxcl2 neutralization
698 antibodies (5ug/ml) treatment. **F,** Quantification of E (n=3). *, $p < 0.05$. **, $p < 0.01$. ***, $p <$
699 $0.001$.

700

701

702

703

704

705

706

707

708

709

710

711 **Figure S6. Correlation analysis of PLK1 and MHC-II genes.**

712 Patients' data ($Log_2^{RSEM}$) are collected from TCGA-LUAD. $r_s$, spearman coefficient.

713

714

715

716

717

718

719

720

721

722

723

724

725

726

727

728

729 **Reference**


730 1. Siegel, R.L., et al., *Cancer statistics, 2023.* CA Cancer J Clin, 2023. **73**(1): p. 17-48.

731 2. Travis, W.D., et al., *International association for the study of lung cancer/american*
732 *thoracic society/european respiratory society international multidisciplinary classification*
733 *of lung adenocarcinoma.* J Thorac Oncol, 2011. **6**(2): p. 244-85.

734 3. Devarakonda, S., D. Morgensztern, and R. Govindan, *Genomic alterations in lung*
735 *adenocarcinoma.* Lancet Oncol, 2015. **16**(7): p. e342-51.

736 4. Doroshow, D.B., et al., *Immunotherapy in Non-Small Cell Lung Cancer: Facts and Hopes.*
737 Clin Cancer Res, 2019. **25**(15): p. 4592-4602.

738 5. Altorki, N.K., et al., *The lung microenvironment: an important regulator of tumour growth*
739 *and metastasis.* Nat Rev Cancer, 2019. **19**(1): p. 9-31.

740 6. Sharma, P. and J.P. Allison, *Immune checkpoint targeting in cancer therapy: toward*
741 *combination strategies with curative potential.* Cell, 2015. **161**(2): p. 205-14.

742 7. Hellmann, M.D., et al., *Nivolumab plus Ipilimumab in Lung Cancer with a High Tumor*
743 *Mutational Burden.* N Engl J Med, 2018. **378**(22): p. 2093-2104.

744 8. Gandhi, L., et al., *Pembrolizumab plus Chemotherapy in Metastatic Non-Small-Cell Lung*
745 *Cancer.* N Engl J Med, 2018. **378**(22): p. 2078-2092.

746 9. Seki, A., et al., *Bora and the kinase Aurora a cooperatively activate the kinase Plk1 and*
747 *control mitotic entry.* Science, 2008. **320**(5883): p. 1655-8.

748 10. Golsteyn, R.M., et al., *Cell cycle regulation of the activity and subcellular localization of*
749 *Plk1, a human protein kinase implicated in mitotic spindle function.* J Cell Biol, 1995.
750 **129**(6): p. 1617-28.

751 11. Elowe, S., et al., *Tension-sensitive Plk1 phosphorylation on BubR1 regulates the stability*
752 *of kinetochore microtubule interactions.* Genes Dev, 2007. **21**(17): p. 2205-19.
753 12. Lane, H.A. and E.A. Nigg, *Antibody microinjection reveals an essential role for human*
754 *polo-like kinase 1 (Plk1) in the functional maturation of mitotic centrosomes.* J Cell Biol,
755 1996. **135**(6 Pt 2): p. 1701-13.
756 13. Neef, R., et al., *Phosphorylation of mitotic kinesin-like protein 2 by polo-like kinase 1 is*
757 *required for cytokinesis.* J Cell Biol, 2003. **162**(5): p. 863-75.
758 14. Schmidt, A., et al., *Xenopus polo-like kinase Plx1 regulates XErp1, a novel inhibitor of*
759 *APC/C activity.* Genes Dev, 2005. **19**(4): p. 502-13.
760 15. Liu, X.S., B. Song, and X. Liu, *The substrates of Plk1, beyond the functions in mitosis.*
761 Protein Cell, 2010. **1**(11): p. 999-1010.
762 16. Strebhardt, K. and A. Ullrich, *Targeting polo-like kinase 1 for cancer therapy.* Nat Rev
763 Cancer, 2006. **6**(4): p. 321-30.
764 17. Gutteridge, R.E., et al., *Plk1 Inhibitors in Cancer Therapy: From Laboratory to Clinics.*
765 Mol Cancer Ther, 2016. **15**(7): p. 1427-35.
766 18. Shin, S.B., et al., *Active PLK1-driven metastasis is amplified by TGF-β signaling that forms*
767 *a positive feedback loop in non-small cell lung cancer.* Oncogene, 2020. **39**(4): p. 767-785.
768 19. Kong, Y., et al., *The kinase PLK1 promotes the development of Kras/Tp53-mutant lung*
769 *adenocarcinoma through transcriptional activation of the receptor RET.* Sci Signal, 2022.
770 **15**(754): p. eabj4009.
771 20. Reda, M., et al., *Development of a nanoparticle-based immunotherapy targeting PD-L1*
772 *and PLK1 for lung cancer treatment.* Nat Commun, 2022. **13**(1): p. 4261.

773 21. Zhang, Z., et al., *Targeting Plk1 Sensitizes Pancreatic Cancer to Immune Checkpoint*
774 *Therapy.* Cancer Res, 2022. **82**(19): p. 3532-3548.
775 22. DuPage, M., A.L. Dooley, and T. Jacks, *Conditional mouse lung cancer models using*
776 *adenoviral or lentiviral delivery of Cre recombinase.* Nat Protoc, 2009. **4**(7): p. 1064-72.
777 23. McGinnis, C.S., L.M. Murrow, and Z.J. Gartner, *DoubletFinder: Doublet Detection in*
778 *Single-Cell RNA Sequencing Data Using Artificial Nearest Neighbors.* Cell Syst, 2019.
779 **8**(4): p. 329-337.e4.
780 24. Stuart, T., et al., *Comprehensive Integration of Single-Cell Data.* Cell, 2019. **177**(7): p.
781 1888-1902.e21.
782 25. Korsunsky, I., et al., *Fast, sensitive and accurate integration of single-cell data with*
783 *Harmony.* Nat Methods, 2019. **16**(12): p. 1289-1296.
784 26. Love, M.I., W. Huber, and S. Anders, *Moderated estimation of fold change and dispersion*
785 *for RNA-seq data with DESeq2.* Genome Biol, 2014. **15**(12): p. 550.
786 27. Gennady, K., et al., *Fast gene set enrichment analysis.* bioRxiv, 2021: p. 060012.
787 28. Liberzon, A., et al., *The Molecular Signatures Database (MSigDB) hallmark gene set*
788 *collection.* Cell Syst, 2015. **1**(6): p. 417-425.
789 29. Kanehisa, M. and S. Goto, *KEGG: kyoto encyclopedia of genes and genomes.* Nucleic
790 Acids Res, 2000. **28**(1): p. 27-30.
791 30. Szklarczyk, D., et al., *The STRING database in 2023: protein-protein association networks*
792 *and functional enrichment analyses for any sequenced genome of interest.* Nucleic Acids
793 Res, 2023. **51**(D1): p. D638-d646.
794 31. Gao, J., et al., *Integrative analysis of complex cancer genomics and clinical profiles using*
795 *the cBioPortal.* Sci Signal, 2013. **6**(269): p. pl1.

796 32. Cerami, E., et al., *The cBio cancer genomics portal: an open platform for exploring*
797 *multidimensional cancer genomics data.* Cancer Discov, 2012. **2**(5): p. 401-4.
798 33. *Comprehensive molecular profiling of lung adenocarcinoma.* Nature, 2014. **511**(7511): p.
799 543-50.
800 34. Cain, D.W. and J.A. Cidlowski, *Immune regulation by glucocorticoids.* Nat Rev Immunol,
801 2017. **17**(4): p. 233-247.
802 35. Jhunjhunwala, S., C. Hammer, and L. Delamarre, *Antigen presentation in cancer: insights*
803 *into tumour immunogenicity and immune evasion.* Nat Rev Cancer, 2021. **21**(5): p. 298-
804 312.
805 36. de Visser, K.E. and J.A. Joyce, *The evolving tumor microenvironment: From cancer*
806 *initiation to metastatic outgrowth.* Cancer Cell, 2023. **41**(3): p. 374-403.
807 37. Mauer, J., et al., *Signaling by IL-6 promotes alternative activation of macrophages to limit*
808 *endotoxemia and obesity-associated resistance to insulin.* Nat Immunol, 2014. **15**(5): p.
809 423-30.
810 38. Wolpe, S.D., et al., *Macrophages secrete a novel heparin-binding protein with*
811 *inflammatory and neutrophil chemokinetic properties.* J Exp Med, 1988. **167**(2): p. 570-
812 81.
813 39. Murooka, T.T., et al., *CCL5-mediated T-cell chemotaxis involves the initiation of mRNA*
814 *translation through mTOR/4E-BP1.* Blood, 2008. **111**(10): p. 4892-901.
815 40. Zhang, H., et al., *CXCL2/MIF-CXCR2 signaling promotes the recruitment of myeloid-*
816 *derived suppressor cells and is correlated with prognosis in bladder cancer.* Oncogene,
817 2017. **36**(15): p. 2095-2104.

818 41. Hu, J., et al., *Regulation of tumor immune suppression and cancer cell survival by*
819 *CXCL1/2 elevation in glioblastoma multiforme.* Sci Adv, 2021. **7**(5).
820 42. Fan, X., et al., *Murine CXCR1 is a functional receptor for GCP-2/CXCL6 and interleukin-*
821 *8/CXCL8.* J Biol Chem, 2007. **282**(16): p. 11658-66.
822 43. Greene, S., et al., *Inhibition of MDSC Trafficking with SX-682, a CXCR1/2 Inhibitor,*
823 *Enhances NK-Cell Immunotherapy in Head and Neck Cancer Models.* Clin Cancer Res,
824 2020. **26**(6): p. 1420-1431.
825 44. Wollenberg, A., et al., *Expression and function of the mannose receptor CD206 on*
826 *epidermal dendritic cells in inflammatory skin diseases.* J Invest Dermatol, 2002. **118**(2):
827 p. 327-34.
828 45. Johnson, D.B., et al., *Melanoma-specific MHC-II expression represents a tumour-*
829 *autonomous phenotype and predicts response to anti-PD-1/PD-L1 therapy.* Nat Commun,
830 2016. **7**: p. 10582.
831 46. Rodig, S.J., et al., *MHC proteins confer differential sensitivity to CTLA-4 and PD-1*
832 *blockade in untreated metastatic melanoma.* Sci Transl Med, 2018. **10**(450).
833 47. Roemer, M.G.M., et al., *Major Histocompatibility Complex Class II and Programmed*
834 *Death Ligand 1 Expression Predict Outcome After Programmed Death 1 Blockade in*
835 *Classic Hodgkin Lymphoma.* J Clin Oncol, 2018. **36**(10): p. 942-950.
836 48. Alspach, E., et al., *MHC-II neoantigens shape tumour immunity and response to*
837 *immunotherapy.* Nature, 2019. **574**(7780): p. 696-701.
838 49. Axelrod, M.L., et al., *Biological Consequences of MHC-II Expression by Tumor Cells in*
839 *Cancer.* Clin Cancer Res, 2019. **25**(8): p. 2392-2402.

840 50. Restifo, N.P., M.J. Smyth, and A. Snyder, *Acquired resistance to immunotherapy and*
841 *future challenges.* Nat Rev Cancer, 2016. **16**(2): p. 121-6.

842

# Figure 1

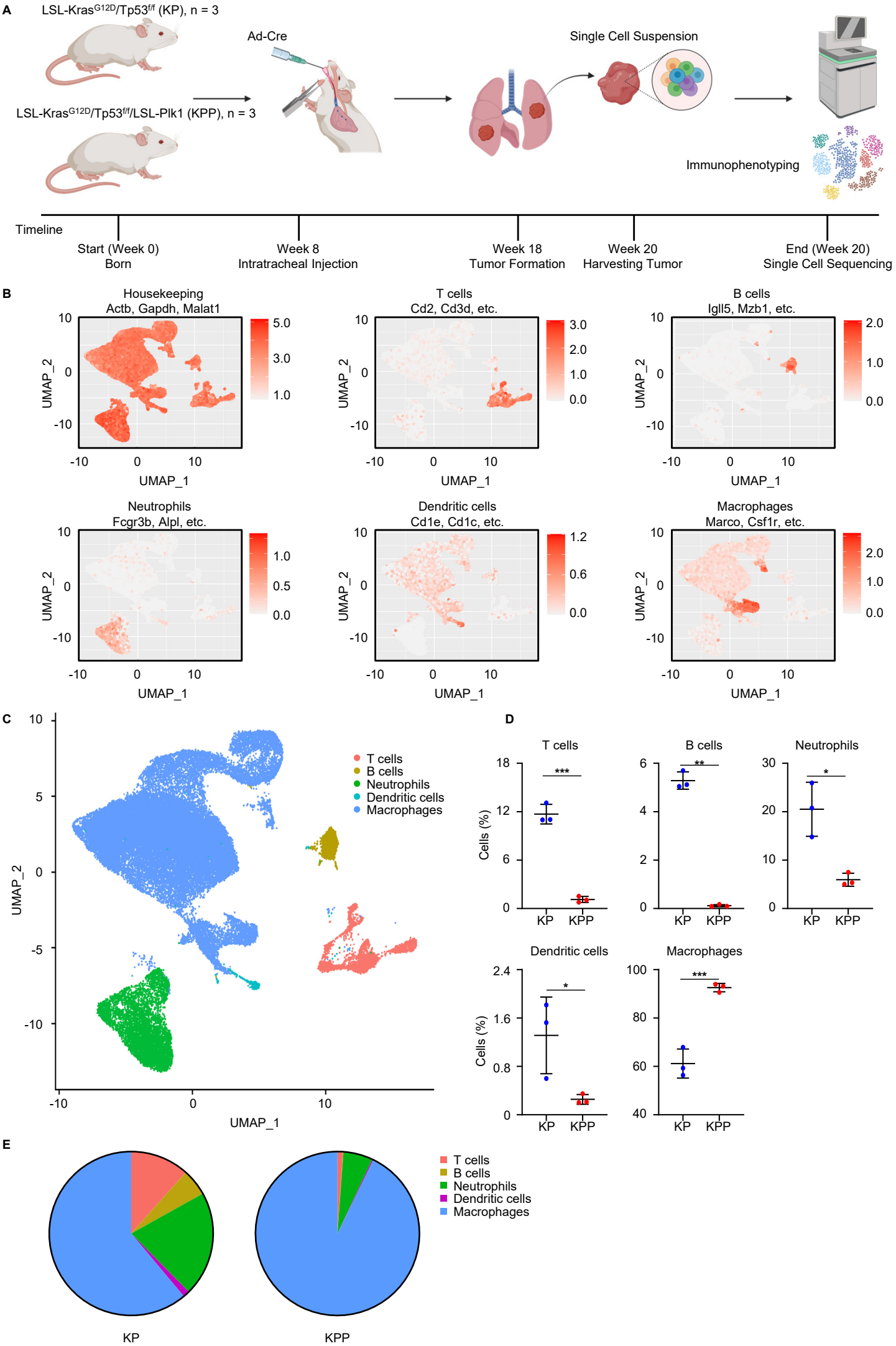
A
LSL-KrasG12D/Tp53f/f (KP), n = 3
LSL-KrasG12D/Tp53f/f/LSL-Plk1 (KPP), n = 3
Ad-Cre
Single Cell Suspension
Immunophenotyping
Timeline
Start (Week 0)
Born
Week 8
Intratracheal Injection
Week 18
Tumor Formation
Week 20
Harvesting Tumor
End (Week 20)
Single Cell Sequencing
B
Housekeeping
Actb, Gapdh, Malat1
T cells
Cd2, Cd3d, etc.
B cells
Igll5, Mzb1, etc.
Neutrophils
Fcgr3b, Alpl, etc.
Dendritic cells
Cd1e, Cd1c, etc.
Macrophages
Marco, Csf1r, etc.
UMAP_1
UMAP_2
C
T cells
B cells
Neutrophils
Dendritic cells
Macrophages
D
Cells (%)
KP
KPP
E
KP
KPP

# Figure 2

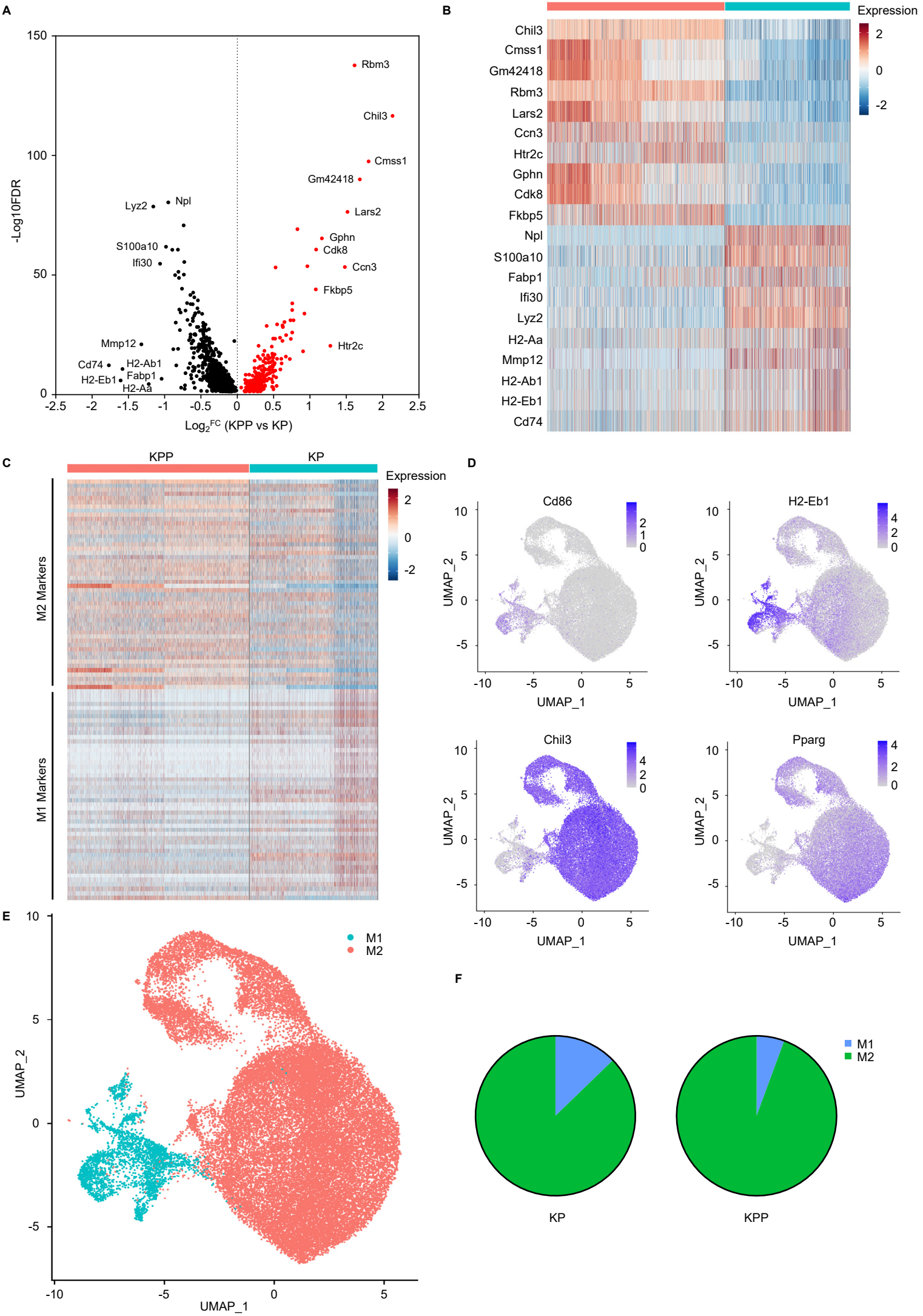
A
-Log10FDR
Log2FC (KPP vs KP)
Rbm3
Chil3
Cmss1
Gm42418
Lars2
Gphn
Cdk8
Ccn3
Fkbp5
Htr2c
Lyz2
Npl
S100a10
Ifi30
Mmp12
Cd74
H2-Ab1
H2-Eb1
Fabp1
H2-Aa
B
KPP
KP
Expression
Chil3
Cmss1
Gm42418
Rbm3
Lars2
Ccn3
Htr2c
Gphn
Cdk8
Fkbp5
Npl
S100a10
Fabp1
Ifi30
Lyz2
H2-Aa
Mmp12
H2-Ab1
H2-Eb1
Cd74
C
KPP
KP
Expression
M2 Markers
M1 Markers
D
Cd86
H2-Eb1
Chil3
Pparg
UMAP_1
UMAP_2
E
M1
M2
UMAP_1
UMAP_2
F
M1
M2
KP
KPP

# Figure 3

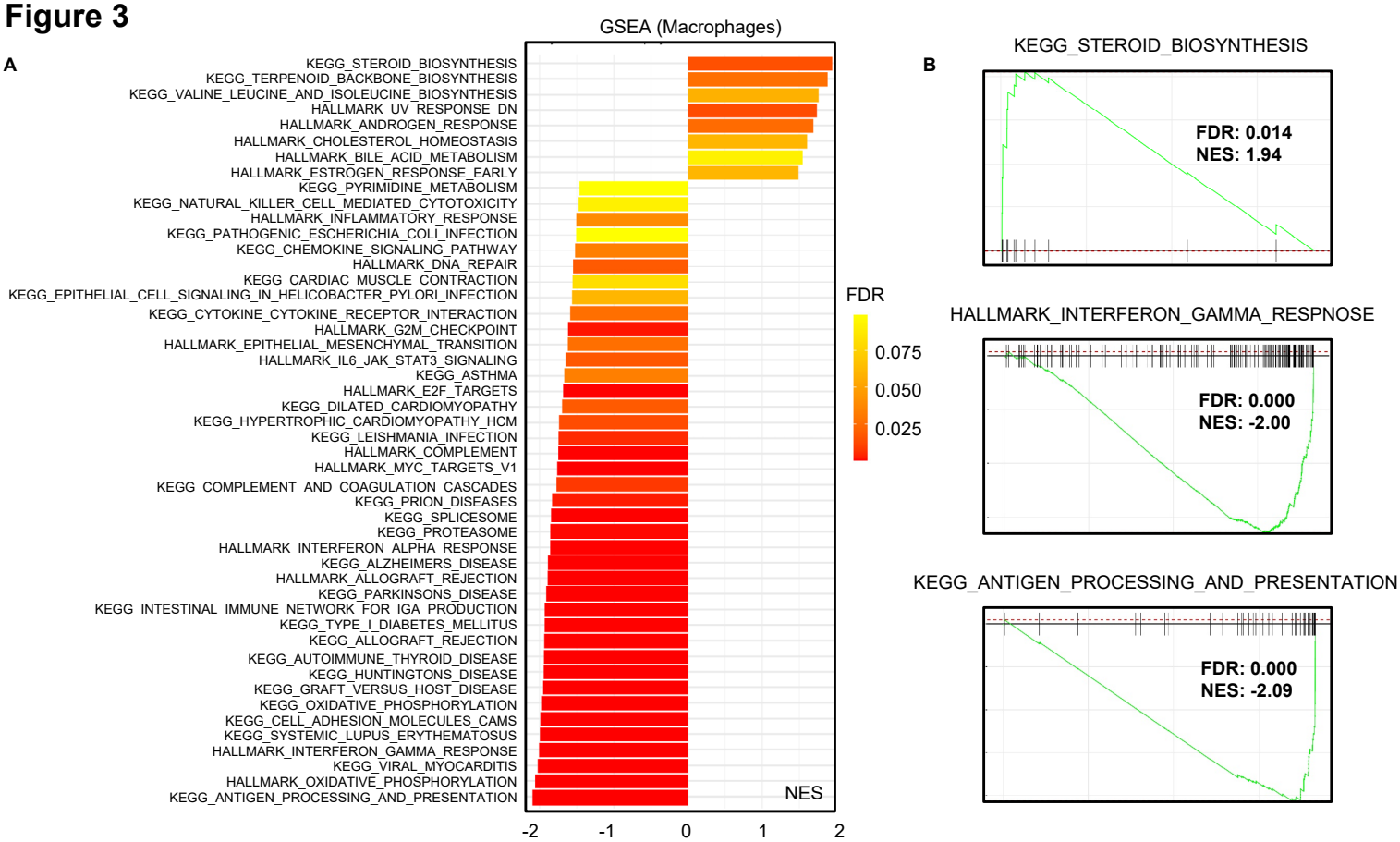
A
GSEA (Macrophages)
KEGG_STEROID_BIOSYNTHESIS
KEGG_TERPENOID_BACKBONE_BIOSYNTHESIS
KEGG_VALINE_LEUCINE_AND_ISOLEUCINE_BIOSYNTHESIS
HALLMARK_UV_RESPONSE_DN
HALLMARK_ANDROGEN_RESPONSE
HALLMARK_CHOLESTEROL_HOMEOSTASIS
HALLMARK_BILE_ACID_METABOLISM
HALLMARK_ESTROGEN_RESPONSE_EARLY
KEGG_PYRIMIDINE_METABOLISM
KEGG_NATURAL_KILLER_CELL_MEDIATED_CYTOTOXICITY
HALLMARK_INFLAMMATORY_RESPONSE
KEGG_PATHOGENIC_ESCHERICHIA_COLI_INFECTION
KEGG_CHEMOKINE_SIGNALING_PATHWAY
HALLMARK_DNA_REPAIR
KEGG_CARDIAC_MUSCLE_CONTRACTION
KEGG_EPITHELIAL_CELL_SIGNALING_IN_HELICOBACTER_PYLORI_INFECTION
KEGG_CYTOKINE_CYTOKINE_RECEPTOR_INTERACTION
HALLMARK_G2M_CHECKPOINT
HALLMARK_EPITHELIAL_MESENCHYMAL_TRANSITION
HALLMARK_IL6_JAK_STAT3_SIGNALING
KEGG_ASTHMA
HALLMARK_E2F_TARGETS
KEGG_DILATED_CARDIOMYOPATHY
KEGG_HYPERTROPHIC_CARDIOMYOPATHY_HCM
KEGG_LEISHMANIA_INFECTION
HALLMARK_COMPLEMENT
HALLMARK_MYC_TARGETS_V1
KEGG_COMPLEMENT_AND_COAGULATION_CASCADES
KEGG_PRION_DISEASES
KEGG_SPLICESOME
KEGG_PROTEASOME
HALLMARK_INTERFERON_ALPHA_RESPONSE
KEGG_ALZHEIMERS_DISEASE
HALLMARK_ALLOGRAFT_REJECTION
KEGG_PARKINSONS_DISEASE
KEGG_INTESTINAL_IMMUNE_NETWORK_FOR_IGA_PRODUCTION
KEGG_TYPE_I_DIABETES_MELLITUS
KEGG_ALLOGRAFT_REJECTION
KEGG_AUTOIMMUNE_THYROID_DISEASE
KEGG_HUNTINGTONS_DISEASE
KEGG_GRAFT_VERSUS_HOST_DISEASE
KEGG_OXIDATIVE_PHOSPHORYLATION
KEGG_CELL_ADHESION_MOLECULES_CAMS
KEGG_SYSTEMIC_LUPUS_ERYTHEMATOSUS
HALLMARK_INTERFERON_GAMMA_RESPONSE
KEGG_VIRAL_MYOCARDITIS
HALLMARK_OXIDATIVE_PHOSPHORYLATION
KEGG_ANTIGEN_PROCESSING_AND_PRESENTATION
NES
-2
-1
0
1
2
FDR
0.075
0.050
0.025
B
KEGG_STEROID_BIOSYNTHESIS
FDR: 0.014
NES: 1.94
HALLMARK_INTERFERON_GAMMA_RESPNOSE
FDR: 0.000
NES: -2.00
KEGG_ANTIGEN_PROCESSING_AND_PRESENTATION
FDR: 0.000
NES: -2.09

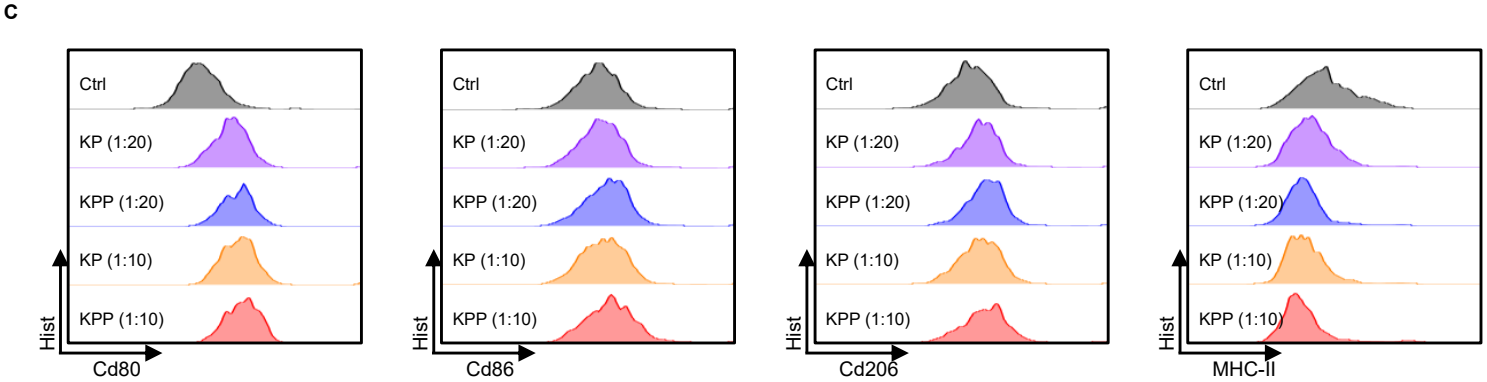
C
Ctrl
KP (1:20)
KPP (1:20)
KP (1:10)
KPP (1:10)
Hist
Cd80
Cd86
Cd206
MHC-II

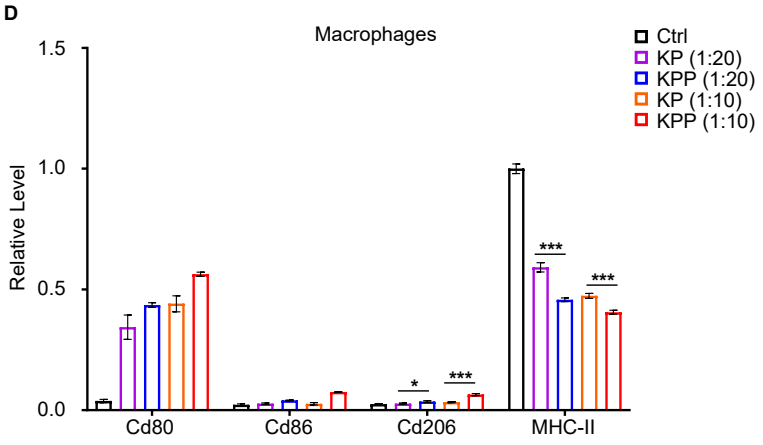
D
Macrophages
Ctrl
KP (1:20)
KPP (1:20)
KP (1:10)
KPP (1:10)
Relative Level
1.5
1.0
0.5
0.0
*
***
Cd80
Cd86
Cd206
MHC-II

# Figure 4

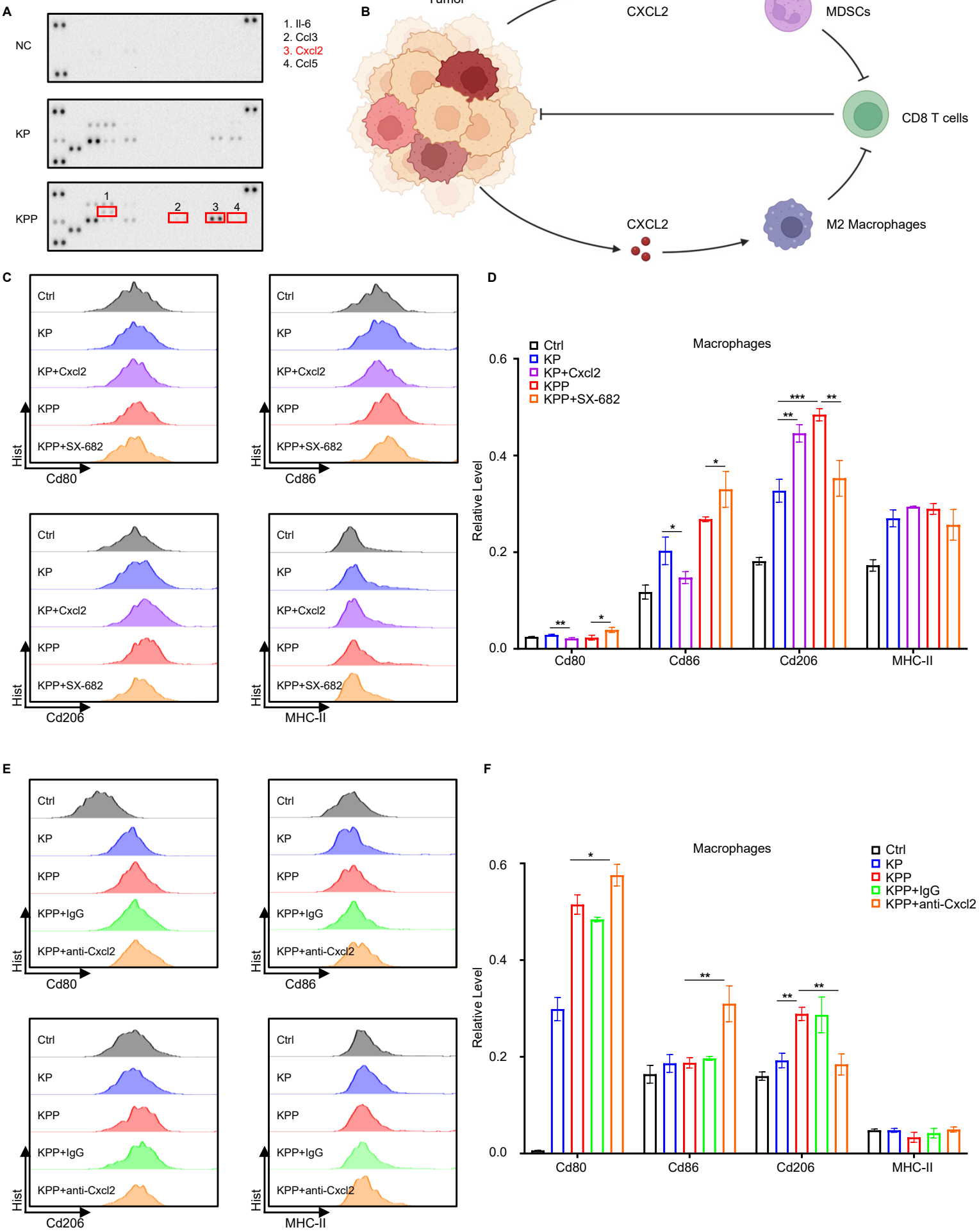
A
NC
KP
KPP
1
2
3
4
1. Il-6
2. Ccl3
3. Cxcl2
4. Ccl5
B
Tumor
CXCL2
MDSCs
CD8 T cells
CXCL2
M2 Macrophages
C
Ctrl
KP
KP+Cxcl2
KPP
KPP+SX-682
Hist
Cd80
Cd86
Cd206
MHC-II
D
Macrophages
Ctrl
KP
KP+Cxcl2
KPP
KPP+SX-682
Relative Level
0.0
0.2
0.4
0.6
Cd80
Cd86
Cd206
MHC-II
E
Ctrl
KP
KPP
KPP+IgG
KPP+anti-Cxcl2
Hist
Cd80
Cd86
Cd206
MHC-II
F
Macrophages
Ctrl
KP
KPP
KPP+IgG
KPP+anti-Cxcl2
Relative Level
0.0
0.2
0.4
0.6
Cd80
Cd86
Cd206
MHC-II

# Figure 5

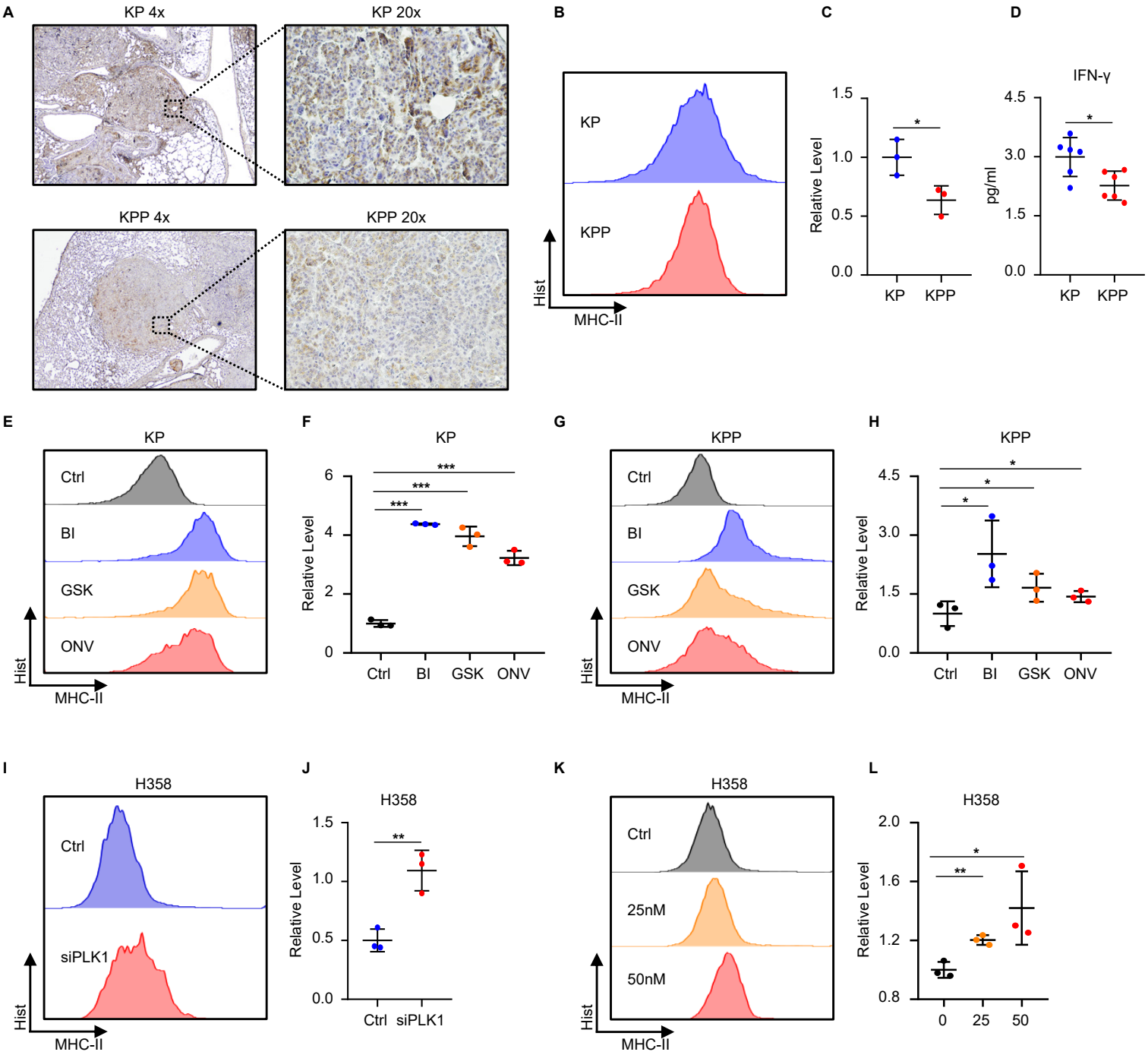
A
KP 4x
KP 20x
KPP 4x
KPP 20x
B
KP
KPP
Hist
MHC-II
C
Relative Level
1.5
1.0
0.5
0.0
*
KP
KPP
D
IFN-γ
pg/ml
4.5
3.0
1.5
0.0
*
KP
KPP
E
KP
Ctrl
BI
GSK
ONV
Hist
MHC-II
F
KP
Relative Level
6
4
2
0
***
***
***
Ctrl
BI
GSK
ONV
G
KPP
Ctrl
BI
GSK
ONV
Hist
MHC-II
H
KPP
Relative Level
4.5
3.0
1.5
0.0
*
*
*
Ctrl
BI
GSK
ONV
I
H358
Ctrl
siPLK1
Hist
MHC-II
J
H358
Relative Level
1.5
1.0
0.5
0.0
**
Ctrl
siPLK1
K
H358
Ctrl
25nM
50nM
Hist
MHC-II
L
H358
Relative Level
2.0
1.6
1.2
0.8
*
**
0
25
50

# Figure 6

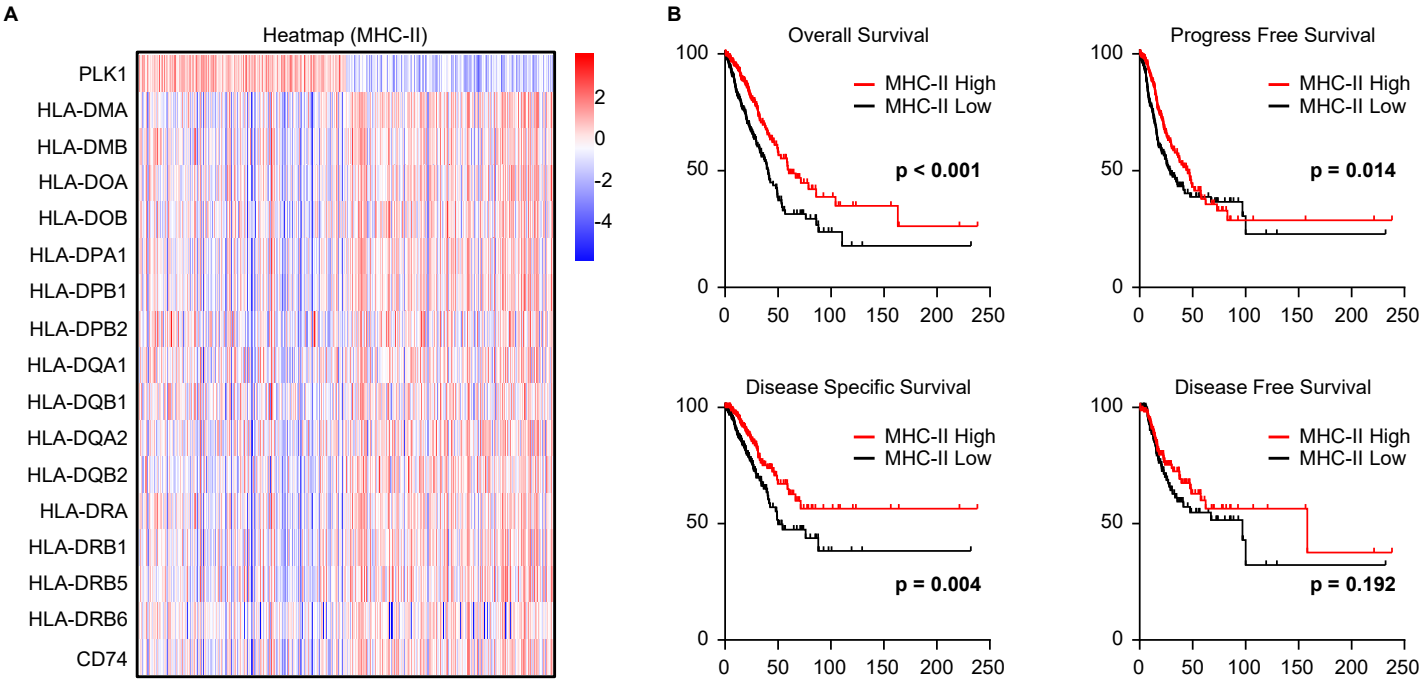
A
Heatmap (MHC-II)
PLK1
HLA-DMA
HLA-DMB
HLA-DOA
HLA-DOB
HLA-DPA1
HLA-DPB1
HLA-DPB2
HLA-DQA1
HLA-DQB1
HLA-DQA2
HLA-DQB2
HLA-DRA
HLA-DRB1
HLA-DRB5
HLA-DRB6
CD74
2
0
-2
-4
B
Overall Survival
MHC-II High
MHC-II Low
p < 0.001
Progress Free Survival
MHC-II High
MHC-II Low
p = 0.014
Disease Specific Survival
MHC-II High
MHC-II Low
p = 0.004
Disease Free Survival
MHC-II High
MHC-II Low
p = 0.192
100
50
0
0
50
100
150
200
250

Figure 7

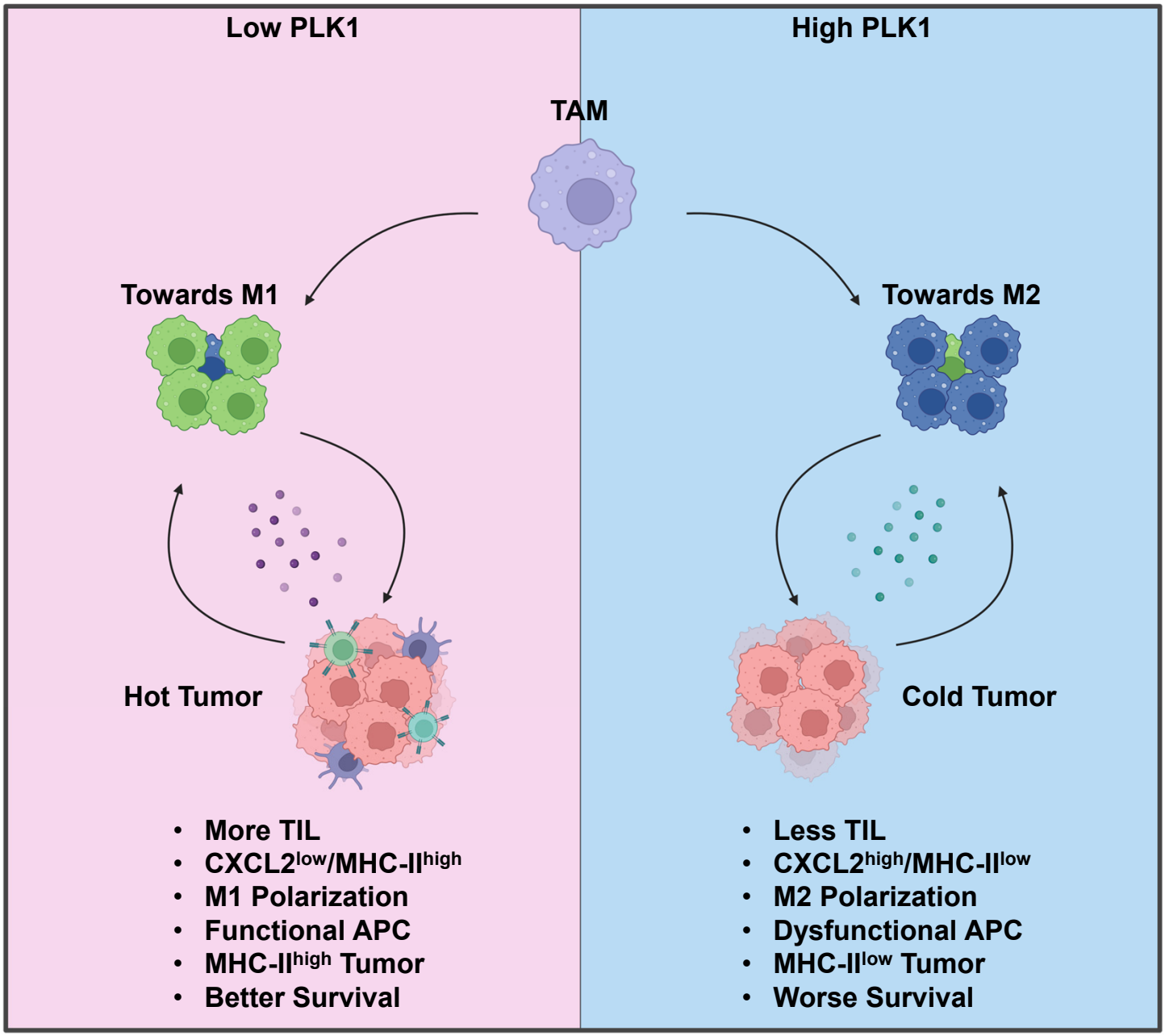
Low PLK1
High PLK1
TAM
Towards M1
Towards M2
Hot Tumor
Cold Tumor
• More TIL
• CXCL2low/MHC-IIhigh
• M1 Polarization
• Functional APC
• MHC-IIhigh Tumor
• Better Survival
• Less TIL
• CXCL2high/MHC-IIlow
• M2 Polarization
• Dysfunctional APC
• MHC-IIlow Tumor
• Worse Survival

# Figure S1

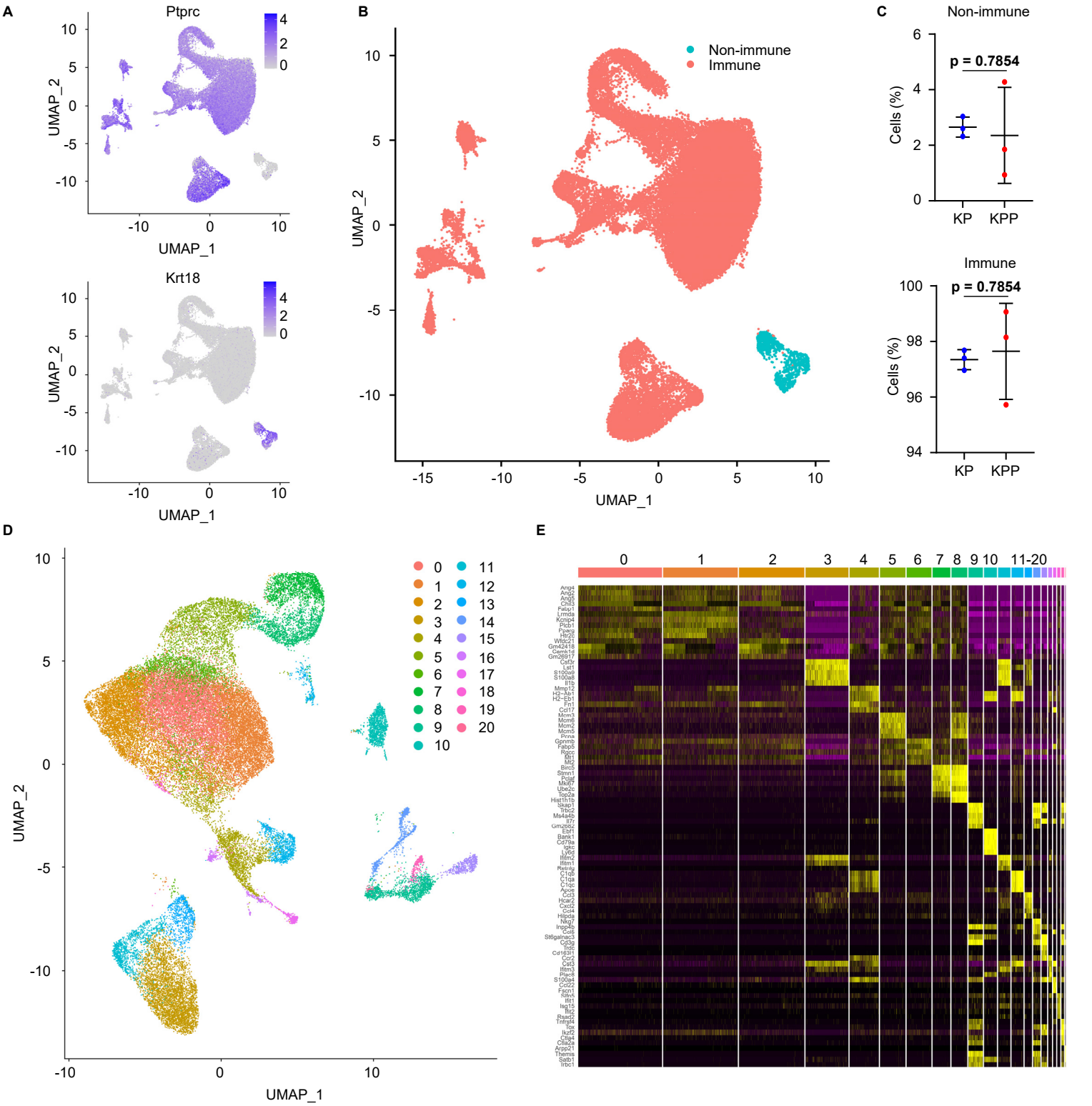
A
Ptprc
Krt18
UMAP_1
UMAP_2
B
Non-immune
Immune
C
Non-immune
Immune
p = 0.7854
Cells (%)
KP
KPP
D
E
F
n=22302
n=23789
Percentage (%)
G
KP
KPP
Percentage (%)

# Figure S2

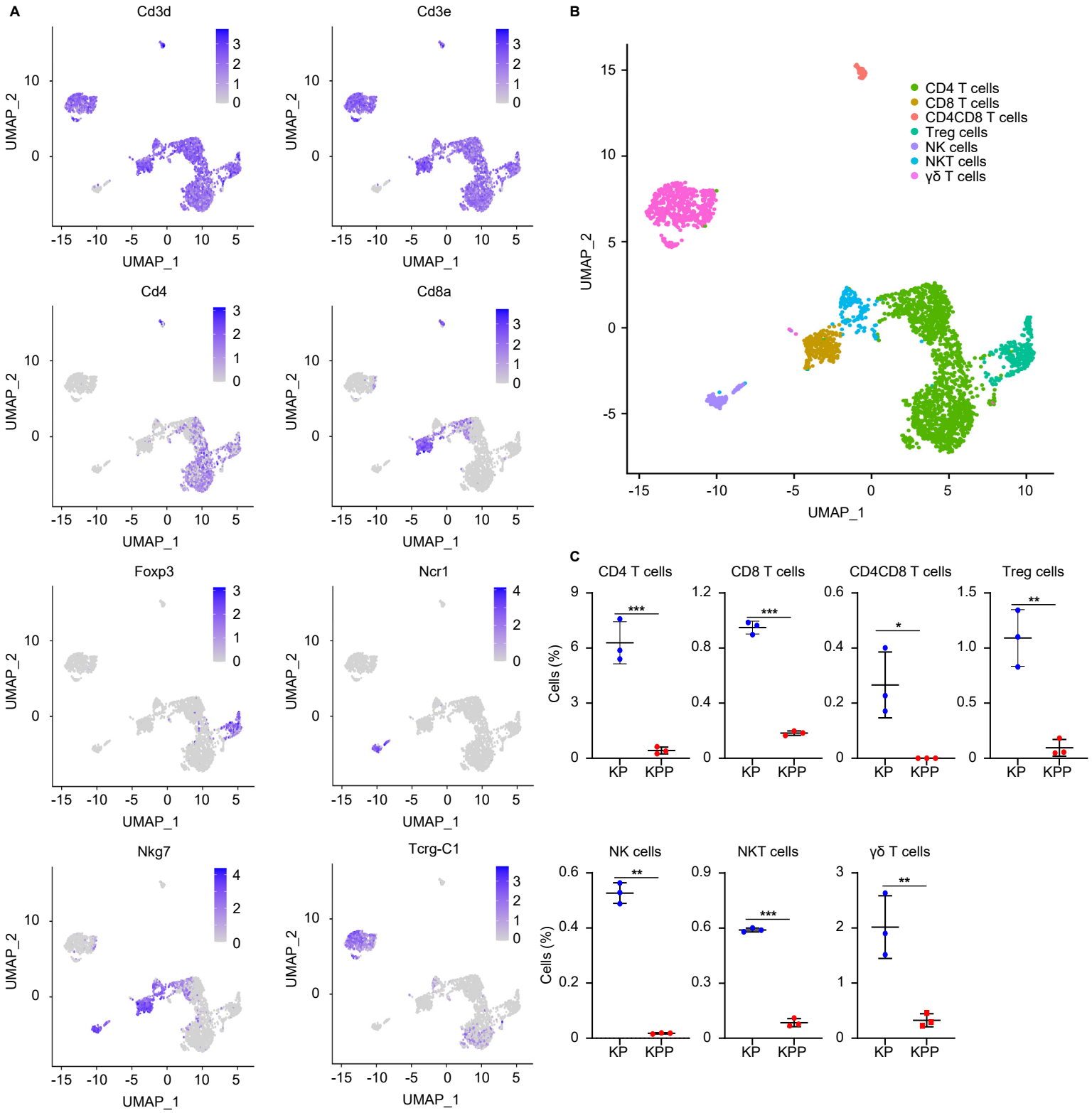
A
Cd3d
Cd3e
Cd4
Cd8a
Foxp3
Ncr1
Nkg7
Tcrg-C1
UMAP_1
UMAP_2
B
CD4 T cells
CD8 T cells
CD4CD8 T cells
Treg cells
NK cells
NKT cells
γδ T cells
C
Cells (%)
KP
KPP

**Figure S3**

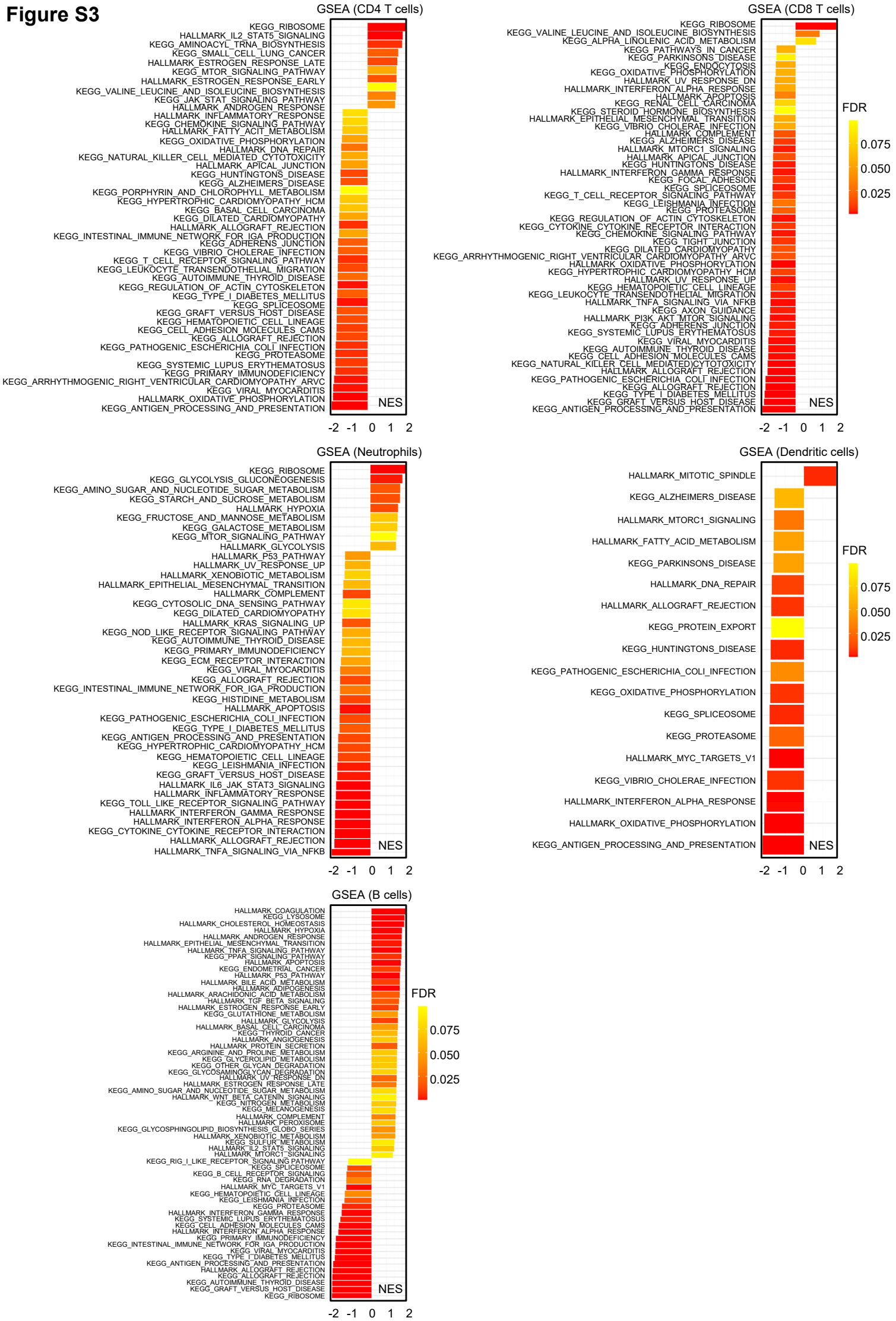
GSEA (CD4 T cells)
KEGG_RIBOSOME
HALLMARK_IL2_STAT5_SIGNALING
KEGG_AMINOACYL_TRNA_BIOSYNTHESIS
KEGG_SMALL_CELL_LUNG_CANCER
HALLMARK_ESTROGEN_RESPONSE_LATE
KEGG_MTOR_SIGNALING_PATHWAY
HALLMARK_ESTROGEN_RESPONSE_EARLY
KEGG_VALINE_LEUCINE_AND_ISOLEUCINE_BIOSYNTHESIS
KEGG_JAK_STAT_SIGNALING_PATHWAY
HALLMARK_ANDROGEN_RESPONSE
HALLMARK_INFLAMMATORY_RESPONSE
KEGG_CHEMOKINE_SIGNALING_PATHWAY
HALLMARK_FATTY_ACIT_METABOLISM
KEGG_OXIDATIVE_PHOSPHORYLATION
HALLMARK_DNA_REPAIR
KEGG_NATURAL_KILLER_CELL_MEDIATED_CYTOTOXICITY
HALLMARK_APICAL_JUNCTION
KEGG_HUNTINGTONS_DISEASE
KEGG_ALZHEIMERS_DISEASE
KEGG_PORPHYRIN_AND_CHLOROPHYLL_METABOLISM
KEGG_HYPERTROPHIC_CARDIOMYOPATHY_HCM
KEGG_BASAL_CELL_CARCINOMA
KEGG_DILATED_CARDIOMYOPATHY
HALLMARK_ALLOGRAFT_REJECTION
KEGG_INTESTINAL_IMMUNE_NETWORK_FOR_IGA_PRODUCTION
KEGG_ADHERENS_JUNCTION
KEGG_VIBRIO_CHOLERAE_INFECTION
KEGG_T_CELL_RECEPTOR_SIGNALING_PATHWAY
KEGG_LEUKOCYTE_TRANSENDOTHELIAL_MIGRATION
KEGG_AUTOIMMUNE_THYROID_DISEASE
KEGG_REGULATION_OF_ACTIN_CYTOSKELETON
KEGG_TYPE_I_DIABETES_MELLITUS
KEGG_SPLICEOSOME
KEGG_GRAFT_VERSUS_HOST_DISEASE
KEGG_HEMATOPOIETIC_CELL_LINEAGE
KEGG_CELL_ADHESION_MOLECULES_CAMS
KEGG_ALLOGRAFT_REJECTION
KEGG_PATHOGENIC_ESCHERICHIA_COLI_INFECTION
KEGG_PROTEASOME
KEGG_SYSTEMIC_LUPUS_ERYTHEMATOSUS
KEGG_PRIMARY_IMMUNODEFICIENCY
KEGG_ARRHYTHMOGENIC_RIGHT_VENTRICULAR_CARDIOMYOPATHY_ARVC
KEGG_VIRAL_MYOCARDITIS
HALLMARK_OXIDATIVE_PHOSPHORYLATION
KEGG_ANTIGEN_PROCESSING_AND_PRESENTATION
NES
-2 -1 0 1 2
GSEA (CD8 T cells)
KEGG_RIBOSOME
KEGG_VALINE_LEUCINE_AND_ISOLEUCINE_BIOSYNTHESIS
KEGG_ALPHA_LINOLENIC_ACID_METABOLISM
KEGG_PATHWAYS_IN_CANCER
KEGG_PARKINSONS_DISEASE
KEGG_ENDOCYTOSIS
KEGG_OXIDATIVE_PHOSPHORYLATION
HALLMARK_UV_RESPONSE_DN
HALLMARK_INTERFERON_ALPHA_RESPONSE
HALLMARK_APOPTOSIS
KEGG_RENAL_CELL_CARCINOMA
KEGG_STEROID_HORMONE_BIOSYNTHESIS
HALLMARK_EPITHELIAL_MESENCHYMAL_TRANSITION
KEGG_VIBRIO_CHOLERAE_INFECTION
HALLMARK_COMPLEMENT
KEGG_ALZHEIMERS_DISEASE
HALLMARK_MTORC1_SIGNALING
HALLMARK_APICAL_JUNCTION
KEGG_HUNTINGTONS_DISEASE
HALLMARK_INTERFERON_GAMMA_RESPONSE
KEGG_FOCAL_ADHESION
KEGG_SPLICEOSOME
KEGG_T_CELL_RECEPTOR_SIGNALING_PATHWAY
KEGG_LEISHMANIA_INFECTION
KEGG_PROTEASOME
KEGG_REGULATION_OF_ACTIN_CYTOSKELETON
KEGG_CYTOKINE_CYTOKINE_RECEPTOR_INTERACTION
KEGG_CHEMOKINE_SIGNALING_PATHWAY
KEGG_TIGHT_JUNCTION
KEGG_DILATED_CARDIOMYOPATHY
KEGG_ARRHYTHMOGENIC_RIGHT_VENTRICULAR_CARDIOMYOPATHY_ARVC
HALLMARK_OXIDATIVE_PHOSPHORYLATION
KEGG_HYPERTROPHIC_CARDIOMYOPATHY_HCM
HALLMARK_UV_RESPONSE_UP
KEGG_HEMATOPOIETIC_CELL_LINEAGE
KEGG_LEUKOCYTE_TRANSENDOTHELIAL_MIGRATION
HALLMARK_TNFA_SIGNALING_VIA_NFKB
KEGG_AXON_GUIDANCE
HALLMARK_PI3K_AKT_MTOR_SIGNALING
KEGG_ADHERENS_JUNCTION
KEGG_SYSTEMIC_LUPUS_ERYTHEMATOSUS
KEGG_VIRAL_MYOCARDITIS
KEGG_AUTOIMMUNE_THYROID_DISEASE
KEGG_CELL_ADHESION_MOLECULES_CAMS
KEGG_NATURAL_KILLER_CELL_MEDIATED)CYTOTOXICITY
HALLMARK_ALLOGRAFT_REJECTION
KEGG_PATHOGENIC_ESCHERICHIA_COLI_INFECTION
KEGG_ALLOGRAFT_REJECTION
KEGG_TYPE_I_DIABETES_MELLITUS
KEGG_GRAFT_VERSUS_HOST_DISEASE
KEGG_ANTIGEN_PROCESSING_AND_PRESENTATION
FDR
0.075
0.050
0.025
NES
-2 -1 0 1 2
GSEA (Neutrophils)
KEGG_RIBOSOME
KEGG_GLYCOLYSIS_GLUCONEOGENESIS
KEGG_AMINO_SUGAR_AND_NUCLEOTIDE_SUGAR_METABOLISM
KEGG_STARCH_AND_SUCROSE_METABOLISM
HALLMARK_HYPOXIA
KEGG_FRUCTOSE_AND_MANNOSE_METABOLISM
KEGG_GALACTOSE_METABOLISM
KEGG_MTOR_SIGNALING_PATHWAY
HALLMARK_GLYCOLYSIS
HALLMARK_P53_PATHWAY
HALLMARK_UV_RESPONSE_UP
HALLMARK_XENOBIOTIC_METABOLISM
HALLMARK_EPITHELIAL_MESENCHYMAL_TRANSITION
HALLMARK_COMPLEMENT
KEGG_CYTOSOLIC_DNA_SENSING_PATHWAY
KEGG_DILATED_CARDIOMYOPATHY
HALLMARK_KRAS_SIGNALING_UP
KEGG_NOD_LIKE_RECEPTOR_SIGNALING_PATHWAY
KEGG_AUTOIMMUNE_THYROID_DISEASE
KEGG_PRIMARY_IMMUNODEFICIENCY
KEGG_ECM_RECEPTOR_INTERACTION
KEGG_VIRAL_MYOCARDITIS
KEGG_ALLOGRAFT_REJECTION
KEGG_INTESTINAL_IMMUNE_NETWORK_FOR_IGA_PRODUCTION
KEGG_HISTIDINE_METABOLISM
HALLMARK_APOPTOSIS
KEGG_PATHOGENIC_ESCHERICHIA_COLI_INFECTION
KEGG_TYPE_I_DIABETES_MELLITUS
KEGG_ANTIGEN_PROCESSING_AND_PRESENTATION
KEGG_HYPERTROPHIC_CARDIOMYOPATHY_HCM
KEGG_HEMATOPOIETIC_CELL_LINEAGE
KEGG_LEISHMANIA_INFECTION
KEGG_GRAFT_VERSUS_HOST_DISEASE
HALLMARK_IL6_JAK_STAT3_SIGNALING
HALLMARK_INFLAMMATORY_RESPONSE
KEGG_TOLL_LIKE_RECEPTOR_SIGNALING_PATHWAY
HALLMARK_INTERFERON_GAMMA_RESPONSE
HALLMARK_INTERFERON_ALPHA_RESPONSE
KEGG_CYTOKINE_CYTOKINE_RECEPTOR_INTERACTION
HALLMARK_ALLOGRAFT_REJECTION
HALLMARK_TNFA_SIGNALING_VIA_NFKB
NES
-2 -1 0 1 2
GSEA (Dendritic cells)
HALLMARK_MITOTIC_SPINDLE
KEGG_ALZHEIMERS_DISEASE
HALLMARK_MTORC1_SIGNALING
HALLMARK_FATTY_ACID_METABOLISM
KEGG_PARKINSONS_DISEASE
HALLMARK_DNA_REPAIR
HALLMARK_ALLOGRAFT_REJECTION
KEGG_PROTEIN_EXPORT
KEGG_HUNTINGTONS_DISEASE
KEGG_PATHOGENIC_ESCHERICHIA_COLI_INFECTION
KEGG_OXIDATIVE_PHOSPHORYLATION
KEGG_SPLICEOSOME
KEGG_PROTEASOME
HALLMARK_MYC_TARGETS_V1
KEGG_VIBRIO_CHOLERAE_INFECTION
HALLMARK_INTERFERON_ALPHA_RESPONSE
HALLMARK_OXIDATIVE_PHOSPHORYLATION
KEGG_ANTIGEN_PROCESSING_AND_PRESENTATION
FDR
0.075
0.050
0.025
NES
-2 -1 0 1 2
GSEA (B cells)
HALLMARK_COAGULATION
KEGG_LYSOSOME
HALLMARK_CHOLESTEROL_HOMEOSTASIS
HALLMARK_HYPOXIA
HALLMARK_ANDROGEN_RESPONSE
HALLMARK_EPITHELIAL_MESENCHYMAL_TRANSITION
HALLMARK_TNFA_SIGNALING_PATHWAY
KEGG_PPAR_SIGNALING_PATHWAY
HALLMARK_APOPTOSIS
KEGG_ENDOMETRIAL_CANCER
HALLMARK_P53_PATHWAY
HALLMARK_BILE_ACID_METABOLISM
HALLMARK_ADIPOGENESIS
HALLMARK_ARACHIDONIC_ACID_METABOLISM
HALLMARK_TGF_BETA_SIGNALING
HALLMARK_ESTROGEN_RESPONSE_EARLY
KEGG_GLUTATHIONE_METABOLISM
HALLMARK_GLYCOLYSIS
HALLMARK_BASAL_CELL_CARCINOMA
KEGG_THYROID_CANCER
HALLMARK_ANGIOGENESIS
HALLMARK_PROTEIN_SECRETION
KEGG_ARGININE_AND_PROLINE_METABOLISM
KEGG_GLYCEROLIPID_METABOLISM
KEGG_OTHER_GLYCAN_DEGRADATION
KEGG_GLYCOSAMINOGLYCAN_DEGRADATION
HALLMARK_UV_RESPONSE_DN
HALLMARK_ESTROGEN_RESPONSE_LATE
KEGG_AMINO_SUGAR_AND_NUCLEOTIDE_SUGAR_METABOLISM
HALLMARK_WNT_BETA_CATENIN_SIGNALING
KEGG_NITROGEN_METABOLISM
KEGG_MELANOGENESIS
HALLMARK_COMPLEMENT
HALLMARK_PEROXISOME
KEGG_GLYCOSPHINGOLIPID_BIOSYNTHESIS_GLOBO_SERIES
HALLMARK_XENOBIOTIC_METABOLISM
KEGG_SULFUR_METABOLISM
HALLMARK_IL2_STAT5_SIGNALING
HALLMARK_MTORC1_SIGNALING
KEGG_RIG_I_LIKE_RECEPTOR_SIGNALING_PATHWAY
KEGG_SPLICEOSOME
KEGG_B_CELL_RECEPTOR_SIGNALING
KEGG_RNA_DEGRADATION
HALLMARK_MYC_TARGETS_V1
KEGG_HEMATOPOIETIC_CELL_LINEAGE
KEGG_LEISHMANIA_INFECTION
KEGG_PROTEASOME
HALLMARK_INTERFERON_GAMMA_RESPONSE
KEGG_SYSTEMIC_LUPUS_ERYTHEMATOSUS
KEGG_CELL_ADHESION_MOLECULES_CAMS
HALLMARK_INTERFERON_ALPHA_RESPONSE
KEGG_PRIMARY_IMMUNODEFICIENCY
KEGG_INTESTINAL_IMMUNE_NETWORK_FOR_IGA_PRODUCTION
KEGG_VIRAL_MYOCARDITIS
KEGG_TYPE_I_DIABETES_MELLITUS
KEGG_ANTIGEN_PROCESSING_AND_PRESENTATION
HALLMARK_ALLOGRAFT_REJECTION
KEGG_ALLOGRAFT_REJECTION
KEGG_AUTOIMMUNE_THYROID_DISEASE
KEGG_GRAFT_VERSUS_HOST_DISEASE
KEGG_RIBOSOME
FDR
0.075
0.050
0.025
NES
-2 -1 0 1 2

# Figure S4

**A**

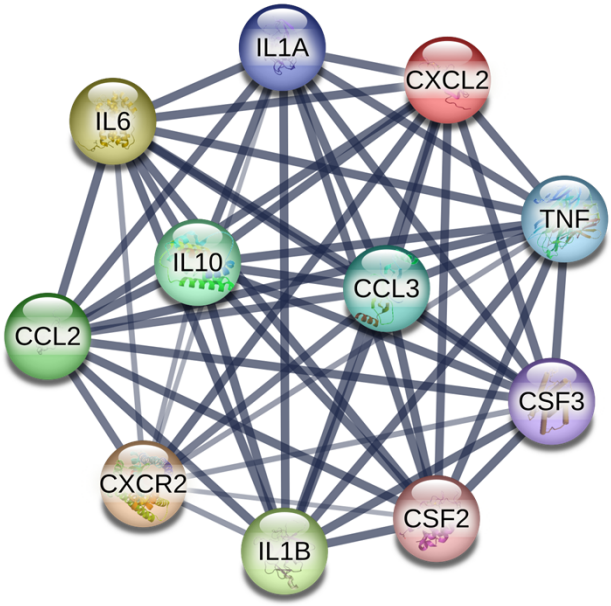


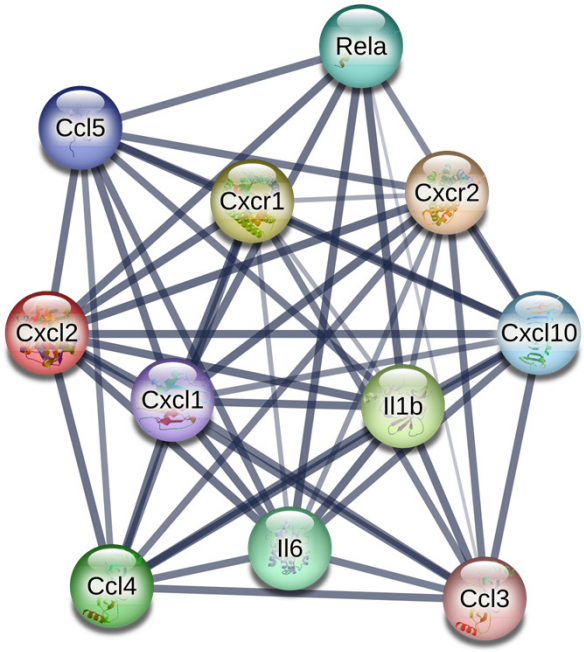


**B**

| GSEA of RNA-seq: GSE206644 (KPP vs KP) | | |
|---|---|---|
| | **HALLMARK_ IL6_JAK_STAT3_SIGNALING** | **HALLMARK_ TNFA_SIGNALING_VIA_NFKB** |
| **NES** | 1.56 | 1.52 |
| **FDR** | **0.023** | **0.028** |

# Figure S5

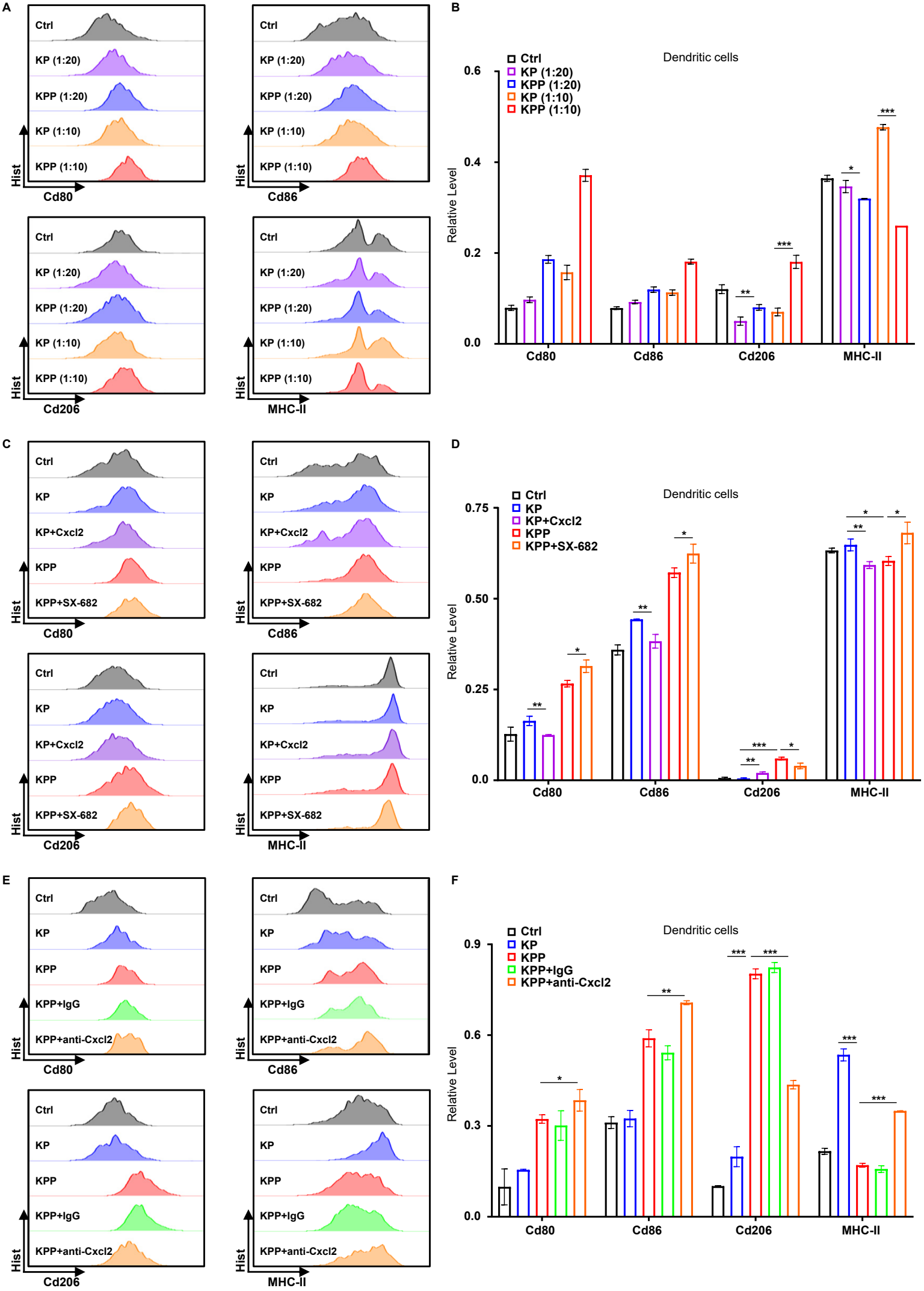
A
Ctrl
KP (1:20)
KPP (1:20)
KP (1:10)
KPP (1:10)
Hist
Cd80
Cd86
Cd206
MHC-II
B
Dendritic cells
Ctrl
KP (1:20)
KPP (1:20)
KP (1:10)
KPP (1:10)
Relative Level
0.0
0.2
0.4
0.6
Cd80
Cd86
Cd206
MHC-II
C
Ctrl
KP
KP+Cxcl2
KPP
KPP+SX-682
Hist
Cd80
Cd86
Cd206
MHC-II
D
Dendritic cells
Ctrl
KP
KP+Cxcl2
KPP
KPP+SX-682
Relative Level
0.0
0.25
0.50
0.75
Cd80
Cd86
Cd206
MHC-II
E
Ctrl
KP
KPP
KPP+IgG
KPP+anti-Cxcl2
Hist
Cd80
Cd86
Cd206
MHC-II
F
Dendritic cells
Ctrl
KP
KPP
KPP+IgG
KPP+anti-Cxcl2
Relative Level
0.0
0.3
0.6
0.9
Cd80
Cd86
Cd206
MHC-II

**Figure S6**

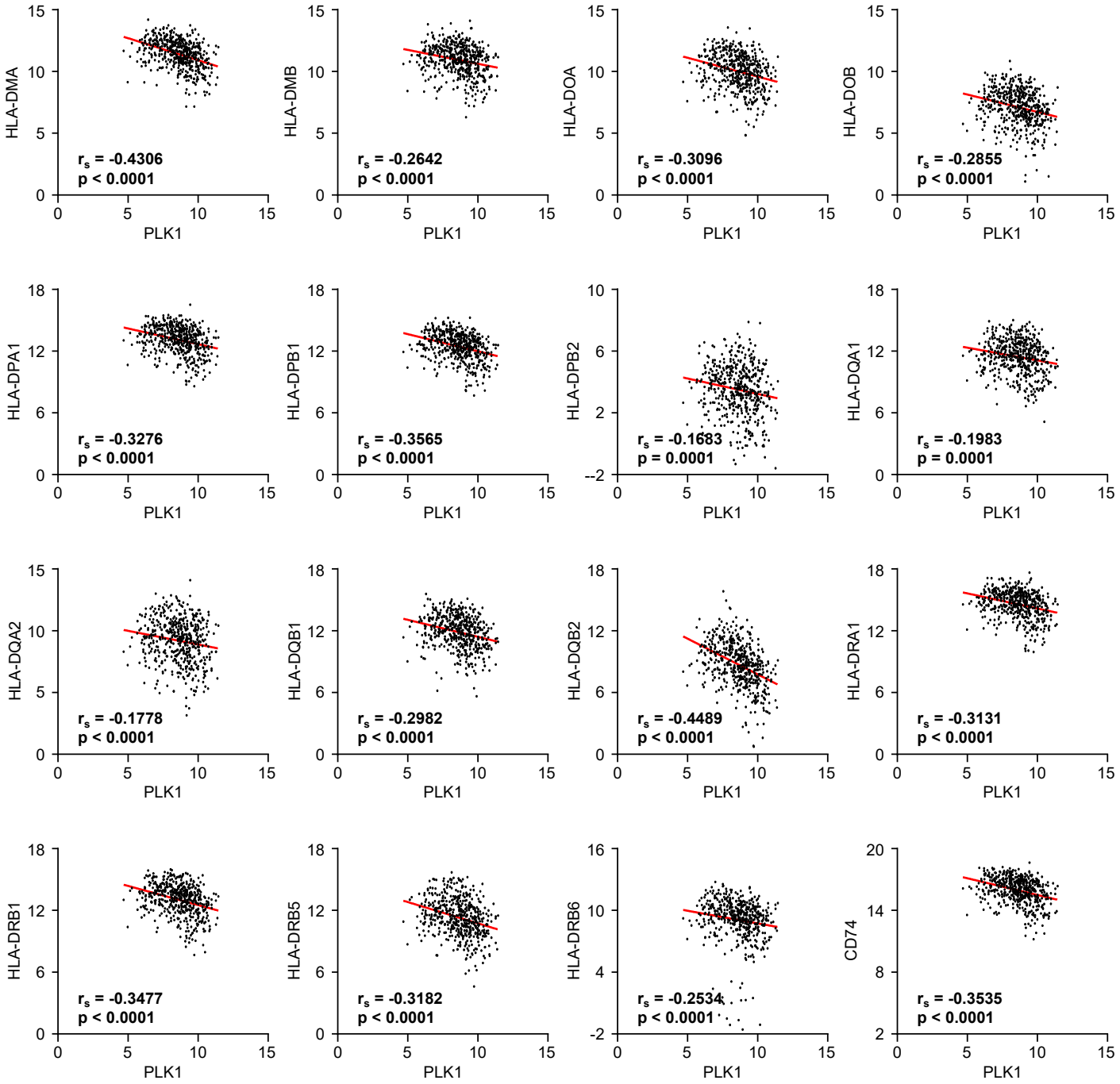
HLA-DMA
$r_s$ = -0.4306
p < 0.0001
HLA-DMB
$r_s$ = -0.2642
p < 0.0001
HLA-DOA
$r_s$ = -0.3096
p < 0.0001
HLA-DOB
$r_s$ = -0.2855
p < 0.0001
HLA-DPA1
$r_s$ = -0.3276
p < 0.0001
HLA-DPB1
$r_s$ = -0.3565
p < 0.0001
HLA-DPB2
$r_s$ = -0.1683
p = 0.0001
HLA-DQA1
$r_s$ = -0.1983
p = 0.0001
HLA-DQA2
$r_s$ = -0.1778
p < 0.0001
HLA-DQB1
$r_s$ = -0.2982
p < 0.0001
HLA-DQB2
$r_s$ = -0.4489
p < 0.0001
HLA-DRA1
$r_s$ = -0.3131
p < 0.0001
HLA-DRB1
$r_s$ = -0.3477
p < 0.0001
HLA-DRB5
$r_s$ = -0.3182
p < 0.0001
HLA-DRB6
$r_s$ = -0.2534
p < 0.0001
CD74
$r_s$ = -0.3535
p < 0.0001
PLK1